

2600-2000  
IN 36-CR  
33459  
p.76

## **Monolith Catalysts for Closed-Cycle Carbon Dioxide Lasers**

Final Report for the Period August 1, 1990 through June 30, 1991

NASA Grant NAG-1-1051

submitted by

Ajay Badlani, Research Assistant, and

\* Richard K. Herz, Associate Professor of Chemical Engineering

Department of Applied Mechanics and Engineering Sciences

University of California, San Diego

La Jolla, California 92093-0310

(\* Principal Investigator)

Grant Technical Officer:

David R. Schryer

NASA Langley Research Center

Hampton, Virginia 23665

(NASA-CP-100725) MONOLITH CATALYSTS FOR  
CLOSED-CYCLE CARBON DIOXIDE LASERS Final  
Report, 1 Aug. 1990 - 30 Jun. 1991  
(California Univ.) 79 p

CSCL 20F

03/35

N91-30590

Unclass  
0033459

## TABLE OF CONTENTS

	Page
<b>TABLE OF CONTENTS</b> .....	ii
<b>LIST OF TABLES</b> .....	v
<b>LIST OF FIGURES</b> .....	vii
<b>ABSTRACT</b> .....	viii
<b>1. <u>INTRODUCTION</u></b> .....	1
1.1. <u>APPLICATIONS OF CO<sub>2</sub> LASERS</u> .....	1
1.2. <u>PROBLEMS ASSOCIATED WITH CO<sub>2</sub> LASERS</u> .....	3
1.3. <u>OTHER APPLICATIONS OF CO OXIDATION CATALYSTS</u> .....	6
1.4. <u>OBJECTIVE OF THIS WORK</u> .....	8
1.5. <u>PREVIOUS WORK ON GOLD CATALYSTS</u> .....	9
1.6. <u>POSSIBLE WAYS OF MAKING A MONOLITHIC CATALYST</u> ...	10
<b>2. <u>MATERIALS, APPARATUS AND PROCEDURES</u></b> .....	12
2.1. <u>CHEMICALS USED</u> .....	12
2.2. <u>CATALYST PREPARATION</u> .....	12
2.3. <u>PELLET PRESSING</u> .....	13
2.4. <u>BET SURFACE AREA MEASUREMENTS</u> .....	13
2.5. <u>ACTIVITY TESTS</u> .....	16

2.5.1.	<u>TEST REACTOR</u> .....	16
2.5.2.	<u>SAFETY FEATURES IN TEST REACTOR</u> .....	18
2.6.	<u>THERMAL TEST</u> .....	20
2.7.	<u>MECHANICAL TEST</u> .....	20
3.	<b><u>RESULTS AND DISCUSSION</u></b> .....	21
3.1.	<u>TESTS ON POWDER</u> .....	21
3.1.1.	<u>EXPERIMENTS TO DETERMINE EXTERNAL MASS TRANSFER RESISTANCE IN THE SYSTEM</u> .....	21
3.1.2.	<u>SPACE VELOCITY VARIATION AND FIRST- ORDER FIT</u> .....	23
3.1.3.	<u>TEMPERATURE VARIATION AND ACTIVATION ENERGY</u> .....	25
3.1.4.	<u>EXPERIMENTS TO DETERMINE TRUE REACTION RATE CONSTANTS</u> .....	27
3.2.	<u>TESTS ON PELLETS</u> .....	29
3.2.1.	<u>BET SURFACE AREA MEASUREMENTS</u> .....	29
3.2.2.	<u>THERMAL CYCLING</u> .....	31
3.2.3.	<u>MECHANICAL TESTS</u> .....	32
3.2.4.	<u>ACTIVITY TESTS ON PELLETS</u> .....	33

3.2.4.1.	EXPERIMENTS TO DETERMINE EXTERNAL MASS TRANSFER RESISTANCE.....	33
3.2.4.2.	EXPERIMENTS TO DETERMINE APPARENT REACTION RATE ORDER.....	35
3.2.4.3.	EXPERIMENTS TO DETERMINE APPARENT ACTIVATION ENERGY.....	36
3.2.4.4.	THIELE MODULUS ANALYSIS .....	38
4.	<b><u>CONCLUSIONS</u></b> .....	53
5.	<b><u>RECOMMENDATIONS FOR FUTURE WORK</u></b> .....	55
6.	<b><u>REFERENCES</u></b> .....	57
7.	<b><u>APPENDIX</u></b> .....	61
7.1.	<b><u>BET TOTAL SURFACE AREA MEASUREMENTS</u></b> .....	61
7.1.1.	<b><u>PROCEDURE</u></b> .....	61
7.1.2.	<b><u>COMPUTER PROGRAMS</u></b> .....	62
7.2.	<b><u>CO OXIDATION REACTOR</u></b> .....	65
7.2.1.	<b><u>ROUTINE OPERATIONS</u></b> .....	65
7.2.2.	<b><u>EMERGENCY PROCEDURES</u></b> .....	66

## LIST OF TABLES

	Page
TABLE 1. EFFECT OF FLOW RATE ON REACTION RATE AT CONSTANT SPACE VELOCITY .....	23
TABLE 2. EFFECT OF SPACE VELOCITY ON REACTION RATE AT CONSTANT TEMPERATURE .....	24
TABLE 3. EFFECT OF TEMPERATURE ON REACTION RATE .....	26
TABLE 4. EXPERIMENTS TO DETERMINE TRUE REACTION RATE CONSTANT (BATCH B) .....	28
TABLE 5. EXPERIMENTS TO DETERMINE TRUE REACTION RATE CONSTANT (BATCH D) .....	28
TABLE 6. EFFECT OF PELLETIZING FORCE ON SURFACE AREA OF PELLETS (BATCH A) .....	30
TABLE 7. COMPARISON BETWEEN SURFACE AREAS AND REACTION RATE CONSTANT OF VARIOUS BATCHES .....	31
TABLE 8. EFFECT OF PELLETIZING FORCE ON THICKNESS AND DENSITY OF PELLETS (BATCH D) .....	32
TABLE 9. EFFECT OF PELLETIZING FORCE ON CRUSH STRENGTH OF THE PELLETS (BATCH D) .....	33
TABLE 10. EFFECT OF FLOW RATE ON REACTION RATE AT CONSTANT SPACE VELOCITY (BATCH D) .....	34
TABLE 11. EFFECT OF SPACE VELOCITY ON APPARENT REACTION RATE AT CONSTANT TEMPERATURE (BATCH D) .....	35

TABLE 12.	EFFECT OF TEMPERATURE ON THE REACTION RATE AT CONSTANT SPACE VELOCITY (BATCH D).....	36
TABLE 13.	EFFECT OF EPOXY AND STAINLESS STEEL STRIP ON REACTION RATE (BATCH B).....	39
TABLE 14.	EFFECT OF EPOXY, STAINLESS STEEL STRIP AND THICKNESS OF THE PELLET ON THE TRUE AND APPARENT REACTION RATE CONSTANT (BATCH B) ...	40
TABLE 15.	COMPARISON OF THEORETICAL EFFECTIVENESS FACTOR WITH THE EXPERIMENTAL EFFECTIVENESS FACTOR (BATCH B) .....	43
TABLE 16.	COMPARISON OF THEORETICAL CONVERSION WITH EXPERIMENTAL CONVERSION (BATCH B).....	44
TABLE 17.	EFFECT OF EPOXY AND STAINLESS STEEL STRIP ON REACTION RATE (BATCH D) .....	46
TABLE 18.	EFFECT OF PELLETIZING FORCE ON TRUE AND APPARENT REACTION RATE CONSTANTS (BATCH D).....	47
TABLE 19.	COMPARISON OF THEORETICAL EFFECTIVENESS FACTOR WITH EXPERIMENTAL EFFECTIVENESS FACTOR (BATCH D).....	48
TABLE 20.	COMPARISON BETWEEN THEORETICAL AND EXPERIMENTAL EFFECTIVENESS FACTOR WITH EFFECTIVE DIFFUSIVITY CORRECTED FOR POROSITY (BATCH D).....	50
TABLE 21.	COMPARISON BETWEEN THEORETICAL CONVERSION AND EXPERIMENTAL CONVERSION (BATCH D) .....	51

## LIST OF FIGURES

	Page
Figure 1. Closed-cycle CO <sub>2</sub> TEA laser schematic.....	5
Figure 2. BET set up.....	14
Figure 3. Flow diagram of CO oxidation test reactor system.....	17
Figure 4. First order fit for Au/MnO <sub>2</sub> powder .....	25
Figure 5. Activation energy of Au/MnO <sub>2</sub> powder .....	27
Figure 6. First order fit Au/MnO <sub>2</sub> pellets .....	36
Figure 7. Activation energy for Au/MnO <sub>2</sub> pellets.....	38
Figure 8. Variation of conversion with time for bad batch of catalyst.....	52

## ABSTRACT

The objective of this work was to explore ways of making a monolithic form of catalyst for CO<sub>2</sub> lasers. Au/MnO<sub>2</sub> was chosen as the catalyst material to be worked with. The approach chosen was to pelletize the Au/MnO<sub>2</sub> powder and epoxy the pellets to stainless steel sheets as structural supports.

The CO oxidation reaction over Au/MnO<sub>2</sub> powder was found to be first overall, and the reaction rate constant at room temperature was  $4.4 \pm 0.3$  cm<sup>3</sup>/g·s. The activation energy was 5.7 kcal/mol (23 kJ/mol).

The BET surface area of the pellets was found to vary from 125 to 140 m<sup>2</sup>/g between different batches of catalyst. Pellets epoxied to stainless steel strips showed no sign of fracture or dusting when subjected to thermal tests. Pellets can be dropped onto hard surfaces with chipping of edges but not breakage of the pellets. Mechanical strength tests performed on the pellets showed that the crush strength is roughly one-fourth of the pelletizing force.

The apparent activity and apparent activation energy over the pellets were found to be less than over the powdered form of the catalyst. The lower apparent activity and activation energy of the pellets are due to the fact that the internal surface area of a pellet is not exposed to the reactant concentration present in the flowing gas as a result of intrapellet diffusion resistance.

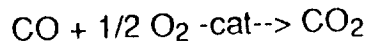
Effectiveness factors varied from 0.44, for pellets having a thickness of 1.1 mm with both faces exposed to the gas, to 0.15 for pellets having thickness of 2 mm and attached with epoxy to a stainless steel strip. The epoxy and the stainless steel strip were found to simply to block off one of the circular faces of

the pellets. The epoxy did not penetrate the pellets and block the active sites. The values of the effective diffusivities were estimated to be between  $2.3 \times 10^{-3}$  and  $4.9 \times 10^{-3} \text{ cm}^2/\text{s}$ . With measurements performed on one powder sample and one pellet configuration, reasonably accurate predictions can be made of conversions that would be obtained with other pellet thickness and configurations.

The results obtained have shown enough promise to further pursue this approach of making monolithic catalysts for  $\text{CO}_2$  laser.

## 1. INTRODUCTION:

The objective of this research is to investigate ways of making monolithic catalysts for closed-cycle transversely excited atmospheric pressure configuration (TEA) CO<sub>2</sub> lasers. The electric discharge used to excite these pulsed CO<sub>2</sub> lasers generally decomposes some of the CO<sub>2</sub>. This decomposition is harmful to long life laser operation both because of the loss of CO<sub>2</sub> and build up of O<sub>2</sub>. Removal of O<sub>2</sub> and replenishment of CO<sub>2</sub> can be achieved in certain applications simply by operating the laser open cycle with continuous flow of fresh laser gas and consequent removal of dissociation products. However, for space-based applications mobile applications or other applications involving weight and/or volume constraints closed-cycle operation with recycling of the laser gas would be imperative. This requires catalytic recombination of the decomposition products, CO and O<sub>2</sub>, to regenerate CO<sub>2</sub>.



### 1.1. APPLICATIONS OF CO<sub>2</sub> TEA LASERS:

Laser remote sensing is a broad area involving both imaging of objects, detection of particles in the air, sensing wind speed and direction and distance ranging (8). Microwave radars are a more conventional method for distance ranging, but lasers offer several advantages based on their shorter wavelength, smaller size beam, lesser beam divergence and beam coherence. Laser radar can create images faster than conventional microwave radars and with the same resolution (8).

The applications of TEA lasers include sensing wind speed and direction, identifying compounds in the atmosphere (by spectra of aerosol backscatter and tracking of hard objects light reflected from the object) (8). Range finding

and targeting are also applications of CO<sub>2</sub> TEA lasers. Remote sensing is useful in military, commercial-aeronautic, and environmental applications.

#### CO<sub>2</sub> LASER BASED PROGRAMS:

##### 1. Laser Atmospheric Wind Sounder (8):

The objective of LAWS is to measure, from space, wind speeds from the surface of the earth up to upper troposphere. LAWS is proposed as one of the earth observing systems (EOS) in NASA's Mission to Planet Earth. The EOS will have different platforms and be cooperative venture with European and Japanese groups. LAWS has been proposed as a primary experimental device for a Japanese polar orbiter to be launched in 1997. The LAWS system is designed to measure wind speeds using aerosol backscatter at different altitudes in 1 km increments. The data obtained can be used for wind field maps in numerical forecasting models to improve long range forecasts.

The atmosphere contains a significant concentration, about 300 ppm of common isotope CO<sub>2</sub> (<sup>12</sup>C<sup>16</sup>O<sub>2</sub>). Common isotope CO<sub>2</sub> cannot be used in the CO<sub>2</sub> laser intended for atmospheric transmission, since the emission frequency resulting from its use would correspond to the absorption frequencies of the atmospheric CO<sub>2</sub>, resulting in poor transmission. Therefore, rare isotope CO<sub>2</sub> (<sup>12</sup>C<sup>18</sup>O<sub>2</sub>) will be used in the LAWS laser. There should be minimum exchange or scrambling of any normal isotope oxygen contained in a catalyst with rare isotope oxygen obtained from dissociation of CO<sub>2</sub> in the laser.

## 2. FIREPOND (8):

This is a Strategic Defense Initiative Organization (SDIO) project. In contrast to LAWS and other wind velocity and aerosol composition experiments this CO<sub>2</sub> laser radar system is used to detect hard objects. The laser radar can collect data on the shape and the rotation speed of the object. The CO<sub>2</sub> laser radar performs range Doppler imaging and images can be taken at ranges between 600 and 750 km and be processed in real time.

## 3. ENVIRONMENTAL AND COMMERCIAL PROGRAMS (8):

Another ground based system that has real time signal processing is in use at the NOAA Wave propagation Laboratories (Boulder, CO). It has been used to measure the transport of pollution. The system has also been used to measure wind velocity around thunderstorms and rough terrains, such as coastlines and mountain valleys. The CO<sub>2</sub> laser used here has advantage over radars in that it can make measurements near the ground. Therefore it can be seen that the pulsed CO<sub>2</sub> lasers have several remote sensing applications both military and non military, which require long life operation with high conversion efficiency and good power stability.

### 1.2. PROBLEMS ASSOCIATED WITH CO<sub>2</sub> LASERS:

CO<sub>2</sub> lasers are normally filled with a gas mixture of N<sub>2</sub>, He and CO<sub>2</sub>. In addition there is always some water vapor present since it is difficult to clean many construction materials (18). The decomposition of CO<sub>2</sub> to CO and O<sub>2</sub> is harmful to long life laser operation both because of the loss of CO<sub>2</sub> and because of the buildup of O<sub>2</sub> (18). The loss of CO<sub>2</sub> results in a corresponding gradual loss of power. The buildup of even relatively small concentrations of

O<sub>2</sub> molecules can cause rapid power loss and even complete laser failure. CO has no deleterious effect on the laser performance at moderate concentrations.

Removal of O<sub>2</sub> and replenishment of CO<sub>2</sub> can be achieved in certain applications simply by operating the laser open cycle with continuous flow through of fresh laser gas and the consequent removal of dissociation products. However for space-based applications or other applications involving weight and/or volume constraints, the amount of gas required for open-cycle operation would be unacceptable and instead, closed laser operation with recycling of the laser gases would be imperative. Achievement of the closed-cycle operation of pulsed CO<sub>2</sub> lasers requires catalytic recombination of the decomposition products, CO and O<sub>2</sub> to regenerate CO<sub>2</sub>. A typical configuration for a closed cycle laser is shown in Figure 1.

Candidate catalysts must have the following features:

1. High efficiency at steady state laser conditions, which are generally 25°C to 100°C and about 1 atm of total pressure with low partial pressures of CO and O<sub>2</sub>.
2. Minimum heating of the catalyst should be required to minimize the power consumption in the laser.
3. The catalyst must be active at stoichiometric ratios of O<sub>2</sub> and CO.
4. It should show no inhibition by CO<sub>2</sub> or other components of the laser environment.
5. It should be thermally and mechanically sound that is it produces no particulates during vibration or thermal cycling.
6. It should have long lifetime with a stable activity.

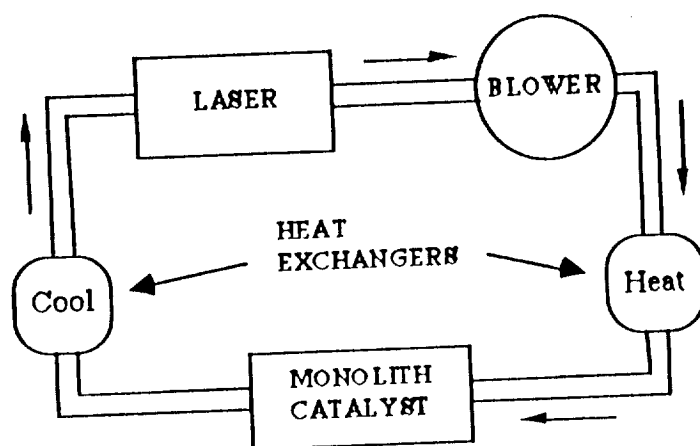


Figure 1. Closed-cycle CO<sub>2</sub> TEA laser schematic

7. There should be minimum exchange or scrambling of any normal isotope oxygen contained in a catalyst with rare isotope oxygen obtained from dissociation of rare isotope  $\text{CO}_2$  in a laser.

### 1.3. OTHER APPLICATIONS OF CO OXIDATION CATALYSTS:

One of the major applications of CO catalysts is removing CO from exhaust of combustion systems. In this emission control application the thermal energy needed to raise the catalyst to operating temperatures is available and excess oxygen which tends to accelerate CO oxidation, is either already present or easily available by injecting air. Both these characteristics are not present in the laser application.

Another major use of CO oxidation catalysts is removing low levels of CO that contaminate breathing air. The CO would be present primarily as the partial oxidation product of combustion process in situations where contamination of breathing air may occur. They are in underground mines, inside burning buildings and aboard submarines. This application differs from laser application in that it has the advantage that there is always excess oxygen available. However it has a disadvantage in common with the laser application in that CO oxidation has to occur at relatively low temperatures. Therefore it can be seen that most the catalyst that are used for applications other  $\text{CO}_2$  lasers are not effective for the  $\text{CO}_2$  lasers.

Catalysts that have been tried as CO oxidation catalysts for  $\text{CO}_2$  lasers include the following: Pt/ $\text{SnO}_2$ , Pd/ $\text{SnO}_2$ , Cu/ $\text{CuO}$ , Pt, Pd/ $\text{SnO}_2$ , Rh/ $\text{SnO}_2$ , Au/ $\text{CeO}$ , Ru/ $\text{MnO}$ , Pt/ $\text{MnO}$ , Au/ $\text{Fe}_2\text{O}_3$  and Au/ $\text{MnO}_2$  (6). These materials fall into a class of catalysts called "noble metal reducible oxide" (NMRO) catalysts (15). This class includes noble metals which are dispersed over a metal

oxide. This metal oxide can be reduced to the parent metal under reaction or pretreatment conditions. In some cases the noble metal can be oxidized and the metal oxide can be converted to a complex compound or alloy.

Conventional noble metal catalysts are dispersed over refractory oxides such as  $\text{Al}_2\text{O}_3$ . The refractory oxide acts as an inert support, that is, it does not participate in the reaction and just provides a means of maintaining high noble metal dispersion (15). CO adsorbed on the noble metal strongly inhibits  $\text{O}_2$  adsorption and thus the reaction proceeds at a slow rate at low temperatures. Over conventional base metal oxide catalysts, oxygen is held too strongly for it to be removed by CO at low temperatures. Since CO and  $\text{O}_2$  have to compete for the same surface sites over noble metals, it is likely that the mixture of two components in the composite NMRO material provides separate sites for CO and  $\text{O}_2$  adsorption (15).

The catalyst used should be in a monolithic form, that is, in a continuous unitary structure. The monolithic form of the catalyst has several advantages over the catalyst used in form of particulate beds. One of the advantages of using the catalyst in the monolithic form, over that in a particulate form, includes design flexibility of the reactor. For example, it is difficult to have a particulate catalyst in a horizontal reactor tube because of the tendency of the catalyst to sag away from the top of the tube, providing a bypass channel. By their nature particulates are free to move when disturbed by pressure surges, shrinkage during the life of the catalyst or other mechanical actions. Therefore special care is taken with fixed bed particulate catalysts to avoid settling or attrition. These precautions include operating the fixed bed in a vertical position with gas flowing down to avoid fluidization. Monolithic reactors can be operated in up flow or down flow and vertically horizontally.

One particularly significant difference between the monolithic and particulate catalysts lies in their pressure drop characteristics. It has been found that the pressure drop for monolithic catalysts are two to three orders of magnitude lower for the same length of bed and flow rate of gas than for comparable particulate systems (41). The lower pressure drop can be achieved without loss in mass transfer conversion efficiencies even at high gas flow rates. This property is the single most important from a reactor design standpoint.

The LASCAT program provides a means to design a monolith catalyst section that will satisfy a user specified set of design requirements (7). The program calculates the bulk average gas temperature, composition and pressure along the length of the monolith. The adjustable parameters required to specify the monolith catalyst section are the monolith dimensions, gas inlet properties and catalyst properties.

#### 1.4. OBJECTIVE OF THIS WORK:

The objective of this work is to explore ways of making a monolithic form of NMRO catalyst materials for CO<sub>2</sub> lasers. Most of the effort related to developing a low temperature CO oxidation catalyst thus far has been expended on platinized tin oxide systems. Although Pt on tin oxide can exhibit considerable CO oxidation activity in this application, acceptable activity is observed if the catalyst undergoes extensive pretreatment. Unfortunately these pretreatments often lead to considerable CO induction periods often lasting several days during which the observed activity declines before reaching a maximum. Even after acceptable activity is recovered these catalysts exhibit steady decay in performance over time. MnO<sub>2</sub> based catalysts are the most active ones

for the oxidation of CO (19). It has been found that the performance of Au/MnO<sub>2</sub> superior to that of Pt/SnO<sub>2</sub> (6) with regard to both catalytic and decay characteristic. Furthermore, the Au/MnO<sub>2</sub> catalyst is less costly than Pt/SnO<sub>2</sub> (6) catalysts. The fact that no pretreatment is required for Au/MnO<sub>2</sub> (6) catalyst is also a significant advantage for Au/MnO<sub>2</sub> catalysts with regard to laser applications (5,6). Therefore Au/MnO<sub>2</sub> was chosen as the catalyst to be investigated.

#### 1.5. PREVIOUS WORK ON GOLD CATALYSTS:

Until now most of the gold catalysts investigated were supported on inactive ceramic oxides, such as SiO<sub>2</sub> (20-26), Al<sub>2</sub>O<sub>3</sub> (23-25), MgO (24-26) and TiO<sub>2</sub> (29), or unsupported gold filaments (30), powder (31, 32), sponges (33), fillings (35) and gauze (36). The chemical reactivity of the gold catalysts has been studied for oxidation by oxygen or nitrogen oxides of CO (10, 20, 31, 33) and H<sub>2</sub> (21, 24, 26, 30-32) selective oxidation of organic compounds by nitrogen dioxide (22), hydrogenation of alkenes (36). The conventional gold catalysts prepared by impregnation have been reported to be far less active for CO and H<sub>2</sub> oxidation by oxygen, than platinum group metal catalyst, though they are superior in selectivity for only a few reactions such as oxidation of 1-pentanol to 1-pentanaldehyde by NO<sub>2</sub> (22) and the hydrogenation of 1-pentene to n-pentane (36). Gold catalysts prepared by coprecipitation from HAuCl<sub>4</sub> and nitrates of various transition metals and calcined in air at 400°C have produced ultrafine gold particles smaller than 10 nm which were uniformly dispersed on the transition metal oxides (12). These catalysts have shown markedly enhanced catalytic activities for CO and H<sub>2</sub> oxidation due to the combined effect of the gold and the transition metal oxides, for example, completely converting

1% CO in air to CO<sub>2</sub> at 30°C at a relative humidity of 76%. They have been found to be active even at -70°C for CO oxidation (10).

#### 1.6. POSSIBLE WAYS OF MAKING A MONOLITHIC CATALYST:

There can be two ways to get Au/MnO<sub>2</sub> in monolithic form. One of techniques involves coprecipitating a mixture of HAuCl<sub>4</sub> and Mn(NO<sub>3</sub>)<sub>2</sub> and then calcining the precipitate to give Au/MnO<sub>2</sub> powder. This powder can then be pressed into pellets and attached to a support structure such as a metal plate.

Another technique involves the simultaneous dispersion of the Au/MnO<sub>2</sub> as it is coprecipitated on a preformed support, for example, a porous ceramic monolith. The process used to develop the catalyst depends upon many factors such as the chemistry of the catalyst components and their possible precursors, the concentration of different components required, the physical strength required, the reaction conditions of the catalyst in use, and the need and ease of removing contaminants. The major advantage of using the first technique over the second technique is that we can start with Au/MnO<sub>2</sub> powder which we know is active. Another advantage of using the first technique is that a uniform distribution of the catalyst can be achieved over the entire monolithic structure.

The major advantage of the second technique is that catalyst developed in this case will have adequate strength since the support can be stabilized to resist reaction conditions before the active phase is incorporated. The major problem with the second technique is the development of the catalyst chemistry.

One of the conclusions from LASCAT studies was that the catalyst layer could be fairly thick because of the relatively low activity of the catalysts com-

pared to automotive monolith catalyst. Therefore one of the ideas to make monolithic catalyst for CO<sub>2</sub> lasers included attaching catalyst pellets to a support such as stainless steel strip. The technique for this work was to press active Au/MnO<sub>2</sub> into pellets and attaching them to a stainless steel strip.

The advantage of pressing the catalyst powder into pellets is that it gives catalyst reasonable strength to withstand attrition in the reactor. The pellets can be attached to rigid support to make it into monolithic form thereby reducing the pressure drop across the reactor and providing flexibility in the design of the reactor. Another reason that motivated the decision to chose the first technique was the fact that development of chemistry for catalyst manufacture could be avoided.

Certain questions that needed to be probed before Au/MnO<sub>2</sub> can be used in a monolithic form in CO<sub>2</sub> lasers. One of the most important question that arises is whether the catalyst can be pressed into pellets that have enough mechanical strength to withstand thermal and mechanical shocks they might be subjected to in the lasers without breaking or shedding particles. Another question that needs to be answered is whether Au/MnO<sub>2</sub> pellets can actually be attached to stainless steel strip. The effect on catalyst activity of the epoxy used to attach the pellets must be explored. Another question which needs to be probed into is whether the pellets have significant internal diffusion resistances.

## **2. MATERIALS, APPARATUS AND PROCEDURES:**

### **2.1. CHEMICALS USED:**

Reagent grade chemicals used for preparation of the catalyst were ordered from Aldrich. The chemical used were:

1. Hydrogen tetrachloroaurate trihydrate ( $\text{HAuCl}_4 \cdot 3\text{H}_2\text{O}$ )
2. Manganese nitrate hexahydrate ( $\text{Mn}(\text{NO}_3)_2 \cdot 3\text{H}_2\text{O}$ )
3. Sodium Carbonate ( $\text{Na}_2\text{CO}_3$ )

### **2.2. CATALYST PREPARATION:**

The catalyst that was prepared is called 10 atom % gold catalyst, since it contains 10 atoms of Au for every 90 atoms of Mn.  $\text{HAuCl}_4 \cdot 3\text{H}_2\text{O}$  is a crystalline powder and is kept in dark. The catalyst was prepared by dissolving 0.8 g of the gold compound (for 10 atom % catalyst) in 250 ml. of water and then dissolving 5.6 g of  $\text{Mn}(\text{NO}_3)_2 \cdot 3\text{H}_2\text{O}$  in a separate container of water. Then 200 ml of 0.5 molar sodium carbonate was added to a precipitation vessel (liter sized beaker). The precipitation vessel was then put over a stirring plate with a Teflon stirring bar in the sodium carbonate solution. The gold and the manganese solutions were then added dropwise over a period of 20 min and the solution was stirred for another 5 min. The stirrer was then turned off and precipitate was allowed to settle. After the solution was decanted off the precipitate, the precipitate was washed three times with 500 ml of distilled water at  $90^\circ\text{C}$ . The precipitate was dried at  $110^\circ\text{C}$  for 21 hours. The dried precipitate was crushed and put in an oven at  $400^\circ\text{C}$  for 4 hours. The catalyst was obtained in form of a powder. This procedure was obtained from Hoflund and Gardner (6).

### 2.3. PELLET PRESSING:

The catalyst powder was pressed into pellets by using a press and a die. The pellets had diameter of 4 mm and, depending upon the mass of the catalyst used, pellets of varying thickness were pressed. The pellets were pressed under a force of 0.5, 1.0 and 1.5 ton. The pellets were attached to the support with Vac Seal epoxy resin obtained from Perkin-Elmer Corporation. The epoxy is designed to seal leaks in stainless steel ultrahigh vacuum chambers, has a bakeout temperature of 150°C, and is usable to  $10^{-9}$  Torr. The epoxy was applied to one of the faces of the pellets and that face of the pellet was pressed down on the stainless strip. The Vac Seal epoxy resin has a set time of 3 hours. The following are the some of its properties:

- |                                      |                          |
|--------------------------------------|--------------------------|
| 1. Viscosity                         | 12000 cps                |
| 2. Operating temperature range:      | -60°C to 150°C           |
| 3. Coefficient of expansion:         | $6 \times 10^5$ cm/cm/°C |
| 4. Water absorption, 30 days at 25°C | 0.18%                    |
| 5. Shelf Life                        | 6 months                 |

### 2.4. BET SURFACE AREA MEASUREMENTS:

Single point BET experiments (38) were performed to determine the surface area of the catalyst. The system used is shown in Figure 2. The catalyst was first outgassed by heating the catalyst to 200°C in flowing He for approximately 20 min and then maintaining the catalyst at a temperature of 200°C for a period of 20 min. The catalyst was then allowed to cool back to room temperature in flowing He. During the process of outgassing the line from the sample cell to the thermal conductivity detector was disconnected to

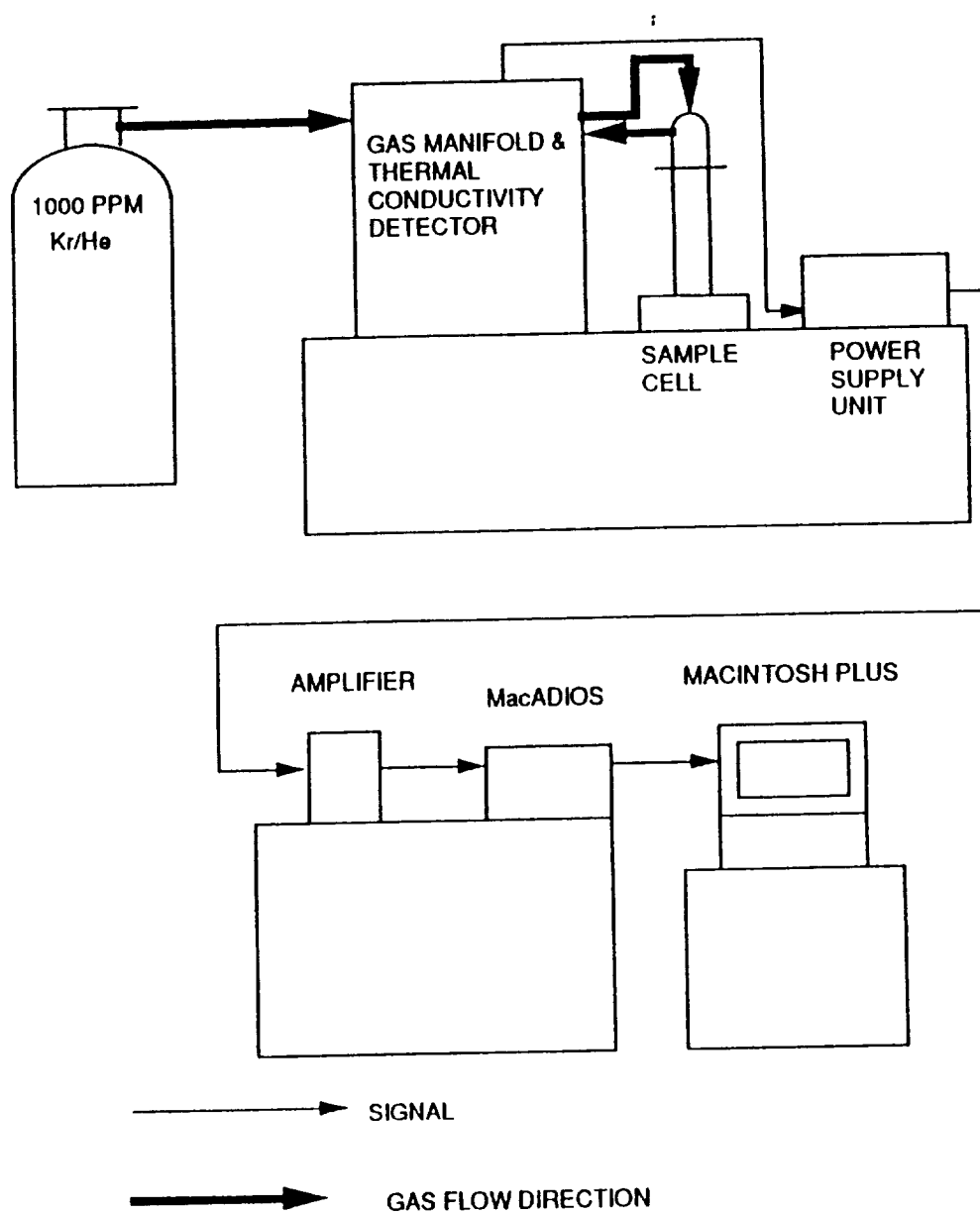


Figure 2. BET set up

prevent the contamination of the thermal conductivity cell with the outgassed water vapor.

A stream of gas composed of the adsorbate (Kr) and inert carrier (He) was passed through the outgassed catalyst. The concentration of the Kr in He was set at a level where the catalyst is covered by an average of about one monolayer of Kr at 77 K. This level corresponds to a relative pressure ( $p/p_0$ ) of 0.3, where  $p$  is the partial pressure of Kr in the sample cell and  $p_0$  (2.0 Torr) is the saturation vapor pressure of Kr at 77K. The composition of gas used in our case was 1000 ppm of Kr in a balance of He. The pressure at the sample cell was 1 atm. The concentration of the adsorbate was continuously monitored by a thermal conductivity cell.

The valves were first set to bypass the sample so that no Kr would adsorb and the thermal conductivity detector could be balanced. The sample cell was then cooled to LN<sub>2</sub> temperature and Kr allowed to adsorb on the catalyst. After sufficient time had elapsed to allow monolayer coverage of the catalyst (40-45 min for samples weighing 10 mg), Kr was desorbed by heating the sample cell to room temperature. Due to desorption there was a change in the concentration of Kr in the gas stream passing through the thermal conductivity cell resulting in a change of signal. The response of the thermal conductivity cell is proportional to the rate of gas desorbing.

The signal from the thermal conductivity cell went to a power supply unit (GOW MAC MODEL 40-200) which transferred it to an amplifier which magnified the signal ten times before passing it to a Macintosh Analog Digital Input Output System (MacADIOS model 411) made by GW instruments. The MacADIOS was interfaced with a Macintosh Plus computer, and data was collected by the computer using a program written in Microsoft Quick BASIC.

Another program written in Quick BASIC then analyzed the data and integrated the peaks obtained. The programs are listed in section 7.1.2 of the appendix. Before determining the surface area of the Au/MnO<sub>2</sub> catalysts, the thermal conductivity cell was first calibrated using aluminum oxide pellets from Alfa Products having a surface area of 100 m<sup>2</sup>/g, per the Alfa catalog.

## 2.5. ACTIVITY TESTS:

### 2.5.1. TEST REACTOR:

Figure 3 is a flow diagram of the test reactor system. The test reactor used was a 1/2 inch O.D. stainless steel tube 5 inches long. A stoichiometric ratio of 1 % CO and 0.5 % O<sub>2</sub> was passed through the test reactor at atmospheric pressure. The reactor was maintained at constant temperature by means of Fisher Isotemp 500 series oven. The concentration of CO<sub>2</sub> was monitored by using a Beckman Industrial infrared analyzer.

The CO<sub>2</sub> infrared analyzer was first calibrated by flowing N<sub>2</sub> through it and adjusting the reading of the analyzer to zero, and then flowing 1% CO<sub>2</sub> in N<sub>2</sub> and adjusting the reading of the analyzer to correspond to 100. The amount of CO<sub>2</sub> formed when the mixture of CO and O<sub>2</sub> was passed through the reactor was obtained from the reading obtained from the analyzer and calibration chart provided by the manufacturer.

The samples that were tested for their activity included catalyst powder, catalyst pellets, catalyst pellets attached to the stainless steel strip by epoxy, and pellets with epoxy applied to only one face of the pellet. The reactor operated as a fixed bed reactor for the powdered form of the catalyst. The reactor also was also made to operate vertically with the gas flowing down to avoid

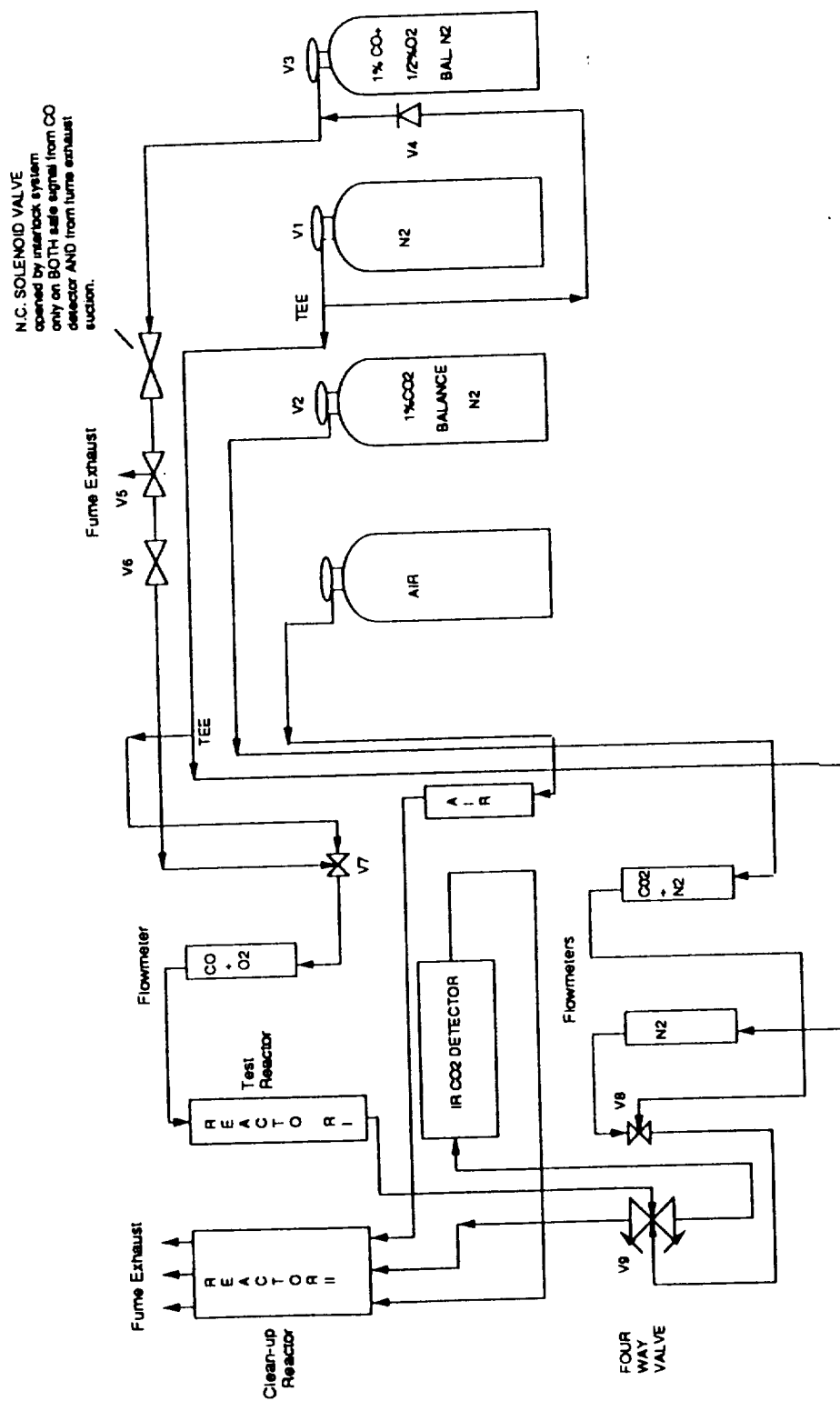


Figure 3. Flow Diagram of CO Oxidation Test Reactor System

fluidization. Pellets were placed so that the circular faces of the pellets were parallel to the gas flow.

### 2.5.2. SAFETY FEATURES IN TEST REACTOR:

CO a colorless, odorless gas with the same specific gravity as that of air. Its inhalation causes asphyxiation by formation of metastable chemical compounds with hemoglobin and biochemical constituents which reduces the availability of oxygen for the cellular systems of the body (37). Due to the toxic nature of CO precautions have to be taken to first avoid any leaks in the system, and, if leaks occur, to detect them. The reactor system used in our case had various types of safety measures to avoid and detect CO leaks in the system. They are:

#### 1. PURGING:

The entire system was purged to remove CO from the system at end of the day. The purge gas used was N<sub>2</sub>. There are three different kinds of purging procedures in the system. They are:

##### A) Purging of the reactor cabinet:

This purge can be done by starting the flow of N<sub>2</sub> through the reactor cabinet by turning valve V7 (Figure 3) to N<sub>2</sub> flow (position 3) and also turning valve V8 to N<sub>2</sub> flow (position 3). This purge should be carried on for 12 min using N<sub>2</sub> flow rates of 20 cm<sup>3</sup>/min. This purges the entire reactor cabinet including the IR analyzer, Reactor I and Reactor II.

**B) Purging the CO regulator:**

This purges the entire gas cabinet and can be performed by starting the flow of  $N_2$  and turning valve V5 (see Figure 3) to position 1 (to vent) and opening valve V4.

**C) Purging the line between the reactor cabinet and the gas cabinet:**

This purge can be performed by turning valve V5 to position 3 (to reactor I) and opening valve V4. Valves V7 and V8 should be turned towards position 3 ( $N_2$  flow) to purge the entire system that is the reactor and the gas cabinet simultaneously.

More details on purging the system are given in section 7.2.1.

**2. INTERLOCK SAFETY MEASURES:**

Interlock safety measures are also provided in the system to prevent CO leaks in the system. The interlock safety system consists of a CO detector system, a normally closed solenoid valve and a relay system. If the level of CO in the surrounding air rises above 100 ppm the detector sounds an alarm and the signal is conveyed to the relay box which opens the circuit and thus closes the solenoid valve, stopping the flow CO to the reactor cabinet. In the above mentioned case both the alarms that is the CO detector alarm and the relay box alarm are triggered on and red light starts blinking on both the detector and the relay box. The relay box also opens the circuit also when the hood fan (exhaust) is not working. In this case both the hood alarm and the alarm in the relay box go on and red light starts blinking on both the

relay box and the hood alarm system. The power to the solenoid valve is thus cut off by the relay box thus closing the solenoid valve and preventing CO from escaping into the exhaust.

## 2.6. THERMAL TEST:

The pellets attached to the stainless steel strip were subjected to thermal cycling. The samples were exposed to temperatures of 100°C and 0°C for a period of 10 min alternatively to check whether the pellets showed signs of cracking or fracture or dusting. The thermal cycling test was repeated ten times.

## 2.7. MECHANICAL TEST:

The pellets pressed under different forces were tested for their crush strength using an Instron machine. A pellet was placed on a fixed flat hard surface and was crushed by applying force through another flat piece that was placed on top of the pellet and that was mobile. The instrument was calibrated to read zero when the upper mobile piece just rested on top of the pellet. The mobile piece was then moved down with levers and the force required to completely crush the pellets was noted.

### 3. RESULTS AND DISCUSSION:

The experiments were performed on four different batches of Au/MnO<sub>2</sub> prepared at different times. Activity tests were performed on both the powdered form of Au/MnO<sub>2</sub> and on pellets. BET, thermal cycling and mechanical tests were also performed on the pellets. Blank tests were performed with no catalyst in the test reactor and the IR detector showed no CO<sub>2</sub> formation for these tests.

Activity tests were performed by passing the gas through the reactor for at least five hours. The conversion of CO to CO<sub>2</sub> remained constant throughout this period. All gas flow rates are given at standard temperature and pressure. The reaction was assumed to take place under isothermal conditions because of the relatively high surface-to-volume ratio of the reactor, low gas flow rates, and low conversions.

#### 3.1. TESTS ON POWDER:

##### 3.1.1. EXPERIMENTS TO DETERMINE EXTERNAL MASS TRANSFER RESISTANCE IN THE SYSTEM:

Experiments to determine external mass transfer resistances were carried out by changing the flow rate of the gas while keeping the ratio of the flow rate to the mass of the catalyst constant. The mass transfer coefficient is generally a function of the velocity of the gas over catalyst particles. For lower velocities the mass transfer boundary layer thickness is large and diffusion limits the reaction. As the velocity over catalyst particles is increased, the boundary layer thickness decreases and the mass transfer across the boundary layer no

longer limits the reaction rate. The mass transfer coefficient for flow and reaction in packed beds is given by (1):

$$k_c = D_{AB} (1-\epsilon) \alpha \{d v / [\mu (1-\epsilon) \alpha] \}^{1/2} (\mu / D_{AB})^{1/3} (d \epsilon)^{-1} \quad (1)$$

where:

$k_c$  = mass transfer coefficient

$d$  = particle diameter (equivalent diameter of sphere of same volume)

$D_{AB}$  = molecular diffusivity

$v$  = superficial gas velocity through the bed

$\mu$  = kinematic viscosity

$\epsilon$  = void fraction of the bed

$\alpha$  = shape factor (external surface area divided by  $\pi d^2$ )

From the above equation it can be seen that, for constant fluid properties and particle diameter,  $k_c \propto v^{1/2}$ . That is the mass transfer coefficient increases with the square root of velocity. Therefore, for a mass transfer limited reaction for the same ratio of mass of the catalyst to the superficial velocity of the gas through the packed bed, the rate of reaction should vary with  $v^{1/2}$ .

Therefore by reducing the velocity of the reactants and the mass of the catalyst in the same proportion, the conversion of CO to CO<sub>2</sub> should be different than obtained for the same ratio of velocity to mass of the catalyst used earlier if there is significant mass transfer resistance in the system. The results obtained were:

TABLE 1. EFFECT OF FLOW RATE ON REACTION RATE AT CONSTANT SPACE VELOCITY (BATCH D)

Experiment	Mass of the catalyst (g)	Flow rate (cm <sup>3</sup> /min)	Space velocity (cm <sup>3</sup> /g·s)	Conversion (%)
1	0.2	70	5.8	56
2	0.1	35	5.8	56

Since no change in the conversion of CO to CO<sub>2</sub> is observed, the assumption of negligible external mass transfer resistance in our system holds for the powdered form of the catalyst.

### 3.1.2. SPACE VELOCITY VARIATION AND FIRST-ORDER FIT:

The experiments below were performed at room temperature. The space velocity of the reactants through the reactor was varied by varying the gas flow rate.

TABLE 2. EFFECT OF SPACE VELOCITY ON REACTION RATE AT  
CONSTANT TEMPERATURE (BATCH C)

Experiment	Mass of the catalyst (g)	Flow rate (cm <sup>3</sup> /min)	Space velocity (cm <sup>3</sup> /g·s)	Conversion (%)
1	0.2	70	5.8	50
2	0.2	55	4.6	55
3	0.2	35	2.9	67

First-order-overall behavior has been reported for the reaction of stoichiometric mixtures of O<sub>2</sub> and CO over tin oxide catalysts (43). That is, the rate is proportional to [O<sub>2</sub>]<sup>a</sup>[CO]<sup>b</sup>, where the orders in O<sub>2</sub> and CO sum to one and [O<sub>2</sub>] = 0.5 [CO] such that the rate is directly proportional to the CO concentration. From the data obtained above it can be verified whether the reaction over Au/MnO<sub>2</sub> shows first-order dependence or not. The plug-flow equation for a first-order isothermal system is given by (17):

$$-\ln(1-x) = \frac{k_{\text{true}}}{(\text{SV})} \quad (2)$$

where

$x$  = fractional conversion of CO to CO<sub>2</sub>

$k_{\text{true}}$  = true reaction rate constant, i.e., measured in absence of mass transport effects

SV = space velocity (q/W)

and where

$W$  = mass of the catalyst

$q$  = gas flow rate

Therefore, for a steady state first-order plug-flow reactor under isothermal conditions and constant  $W$ , a plot of  $-\ln(1-x)$  vs  $1/q$  should give us a straight line.

Figure 4 shows the plot of  $-\ln(1-x)$  vs  $1/q$  for the powdered form of the catalyst obtained from Batch C. The reaction approximates a first-order system well. Therefore the reaction rate is proportional to  $[O_2]^a[CO]^b$ , where sum of  $a$  and  $b$  equals one. The value of the reaction rate constant for Batch C at room temperature was determined to be  $4.6 \text{ cm}^3/\text{g}\cdot\text{s}$ .

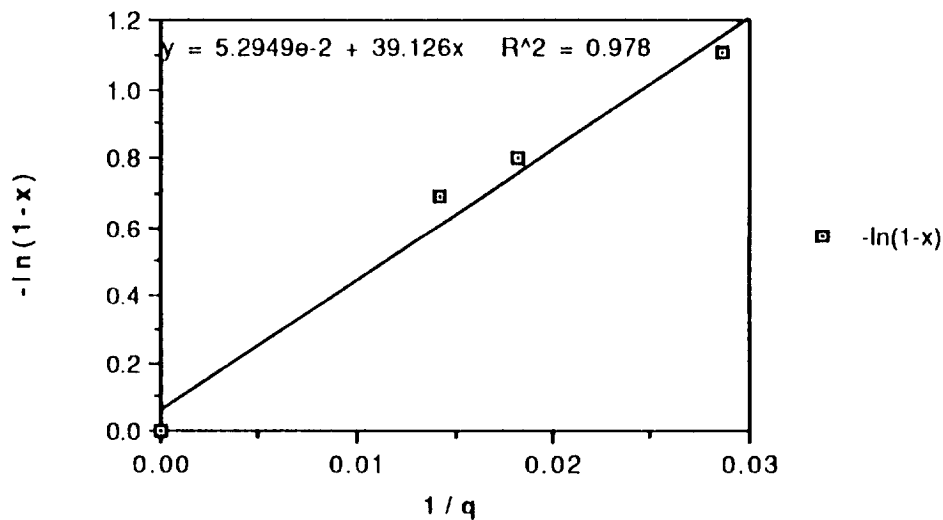


Figure 4. First-order fit for Au/MnO<sub>2</sub> powder

### 3.1.3. TEMPERATURE VARIATION AND ACTIVATION ENERGY:

Experiments to investigate the effect of temperature on conversion were done using a reactant flow rate of 70 cm<sup>3</sup>/min, a catalyst mass of 0.2 grams and, therefore, a space velocity of 5.8 cm<sup>3</sup>/g.s.

TABLE 3. EFFECT OF TEMPERATURE ON REACTION RATE (BATCH C)

Experiment	Mass of the catalyst (g)	Temperature (°C)	Conversion (%)
1	0.20	23	50
2	0.20	34	63
3	0.20	49	74

The dependence of reaction rate constant on temperature is assumed to be based on the Arrhenius reaction rate law:

$$k_{true} = A_{true} \exp(-E_{true} / RT) \quad (3)$$

where:

$k_{true}$  = reaction rate constant

$A_{true}$  = pre-exponential factor

$E_{true}$  = activation energy for the reaction

$T$  = temperature in K at which the reaction is carried out

Taking the natural logarithm of both sides of (3) we get

$$\ln k_{true} = \ln A_{true} - \frac{E_{true}}{RT} \quad (4)$$

Therefore a plot of  $\ln k$  vs  $1/T$  should give a straight line (17). The value of  $k$  is obtained from Equation (1) using the conversion obtained in each case.

Figure 5 shows the dependence of reaction rate constant on temperature. The plot of  $\ln k$  vs  $1/T$  gives a straight line, confirming that the effect of temperature on reaction rate is through an Arrhenius dependence on reaction rate constant. The activation energy for the reaction over Batch C can be determined from the slope of this line and is found to be 5.7 kcal/mol (23 kJ/mol).

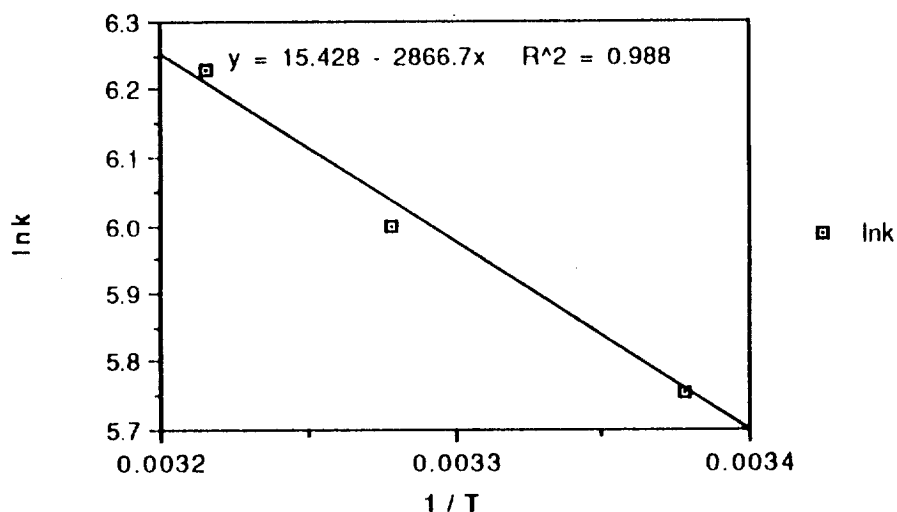


Figure 5. Activation energy of Au/MnO<sub>2</sub> powder

#### 3.1.4. EXPERIMENTS TO DETERMINE TRUE REACTION RATE CONSTANTS:

The following experiments were performed on Batch B of the catalyst. All experiments were performed at room temperature and a reactant flow rate of 70 cm<sup>3</sup>/min. The experiments were performed to determine the true reaction rate constant for this batch of catalyst.

TABLE 4. EXPERIMENTS TO DETERMINE TRUE REACTION RATE  
CONSTANT (BATCH B)

Experiment	Mass of the catalyst (g)	Conversion (%)
1	0.24	61
2	0.24	57
3	0.28	69

The reaction rate constant for Batch B at room temperature was determined to be  $4.6 \text{ cm}^3/\text{g}\cdot\text{s}$ .

Experiments with Batch D of catalyst were performed at flow rates of  $70 \text{ cm}^3/\text{min}$  and at room temperatures. The experiments were performed to determine the true reaction rate constant. The following results were obtained:

TABLE 5. EXPERIMENTS TO DETERMINE TRUE REACTION RATE  
CONSTANT (BATCH D)

Experiment	Mass of the catalyst (g)	Conversion (%)
1	0.2	55
2	0.2	55

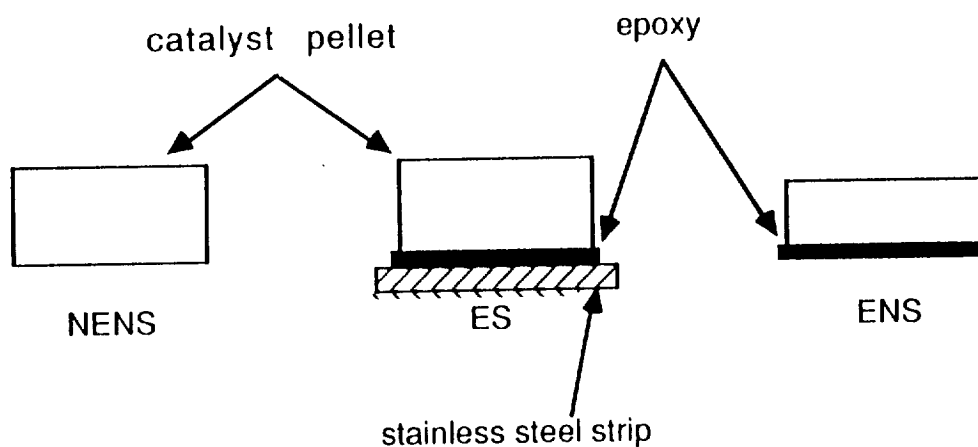
The reaction rate constant for Batch D at room temperature was determined to be  $4.7 \text{ cm}^3/\text{g}\cdot\text{s}$ .

### 3.2. TESTS ON PELLETS:

Three different types of configurations were used while performing tests on pellets. These three kinds of configuration have been abbreviated in the text as follows:

1. NENS: Pellets with no epoxy or strip attached to them.
2. ES: Pellets which were attached to the stainless steel strip with epoxy.
3. ENS: Pellets with epoxy applied to one of the circular faces of the pellets without being attached to the stainless steel strip.

The cross sections of these configurations are, schematically:



#### 3.2.1. BET SURFACE AREA MEASUREMENTS:

BET surface area measurements were performed on batches A, B, D. Experiments performed with catalyst powder gave flat peaks. The flat peaks were due to saturation of one of the instruments used in the surface area measurements. One of the possible reasons for the saturation to occur is that the diffusional resistance in case of powdered form of the catalyst is small. This results in immediate release of adsorbed Kr upon warming and thus, a large

signal from the thermal conductivity detector leading to saturation of one of the instruments.

The effect of force under which the pellets were pressed on the surface area of the pressed pellet was examined with Batch A. The following results were obtained:

TABLE 6. EFFECT OF PELLETIZING FORCE ON SURFACE AREA OF PELLETS (BATCH A)

Pelletizing force (ton, 1 ton = 276 N)	BET surface area (m <sup>2</sup> /g)
0.5	65
1.0	69
2.0	64

The BET experiments performed on this batch of catalyst showed no effect of force under which the pellet is pressed on the surface area of the pellet.

#### BATCH B

The surface area of one of the pellets (pressed under a force of 0.5 ton) was determined. The weight of the sample used was 5.8 mg and its surface area was found to be 150 m<sup>2</sup>/g.

#### BATCH D

The surface area of one of the pellets (pressed under a force of 0.5 ton) was determined and found to be 126 m<sup>2</sup>/g.

Since it was difficult to perform BET experiments with the powdered form of the catalyst, the exact surface area of the powdered form of the catalyst was not known. The surface area of the powder is not expected to differ much from the surface area of the pellets since the surface area of the pellets was found to be independent of the pelletizing force. The results obtained from BET surface area measurements are summarized below:

TABLE 7. COMPARISON BETWEEN SURFACE AREAS AND REACTION RATE CONSTANT OF VARIOUS BATCHES

Batch	BET area of 0.5 ton pellet (m <sup>2</sup> /g)	k <sub>true</sub> (cm <sup>3</sup> /g·s)
A	65	-----
B	150	4.6
D	126	4.7

### 3.2.2. THERMAL CYCLING:

The thermal cycling tests were performed by alternatively subjecting the catalyst pellet to temperatures of 0°C and 100°C for a period of 10 min at each temperature. This process was repeated ten times. These tests were performed on Batch C and the pellets showed no signs of cracking or powder formation during this test.

### 3.2.3. MECHANICAL TESTS:

The thickness of the pellets varied with the force under which the pellets were pressed. For the same mass of the catalyst (0.2 g) the thickness and the density of the pellets varied as follows:

TABLE 8. EFFECT OF PELLETIZING FORCE ON THICKNESS AND DENSITY OF PELLETS (BATCH D)

Pelletizing force (ton, 1 ton = 276 N)	Thickness (mm)	Density (g/cm <sup>3</sup> )
0 (POWDER)	-----	5.90
0.5	2.0	7.96
1.0	1.9	8.38
1.5	1.8	8.85

Mechanical tests were performed on Batches C and D of the catalyst. The crush strength of pellets pressed under forces of 0.5 ton and 1.0 ton and 1.5 ton was determined. The results obtained are as follows:

TABLE 9. EFFECT OF PELLETIZING FORCE ON CRUSH STRENGTH OF THE PELLETS (BATCH D)

Pelletizing force	Pelletizing pressure	Crushing force	Crushing pressure
0.5 ton 138 N	$5.14 \times 10^4 \text{ lb/in}^2$ $3.44 \times 10^8 \text{ N/m}^2$	250 lbs 34.6 N	$1.28 \times 10^4 \text{ lbs/in}^2$ $8.8 \times 10^7 \text{ N/m}^2$
1.0 ton 276 N	$1.02 \times 10^5 \text{ lb/in}^2$ $7.03 \times 10^8 \text{ N/m}^2$	450 lbs 62.2 N	$2.31 \times 10^4 \text{ lbs/in}^2$ $1.59 \times 10^8 \text{ N/m}^2$
1.5 ton 415 N	$1.54 \times 10^5 \text{ lb/in}^2$ $1.06 \times 10^9 \text{ N/m}^2$	750 lbs 104 N	$3.85 \times 10^4 \text{ lbs/in}^2$ $2.65 \times 10^8 \text{ N/m}^2$

The results indicate that the crush strength of the pellets increases with the force under which the pellets were originally pressed. The crush strength is approximately one-fourth of the pelletizing pressure.

#### 3.2.4. ACTIVITY TESTS ON PELLETS:

##### 3.2.4.1. *EXPERIMENTS TO DETERMINE EXTERNAL MASS TRANSFER RESISTANCE:*

Experiments to determine whether external mass transfer resistances were present in the system were carried out by changing the gas flow rate while keeping the space velocity constant. The mass transfer coefficient for laminar flow through a circular tube is given by (39):

$$k_c = 1.86 \left( \frac{d v}{\mu} \right)^{0.8} \left( \frac{D_{AB}}{d} \right) \quad (5)$$

where:

$k_c$  = mass transfer coefficient

$d$  = diameter of the circular tube

$D_{AB}$  = molecular diffusivity

$v$  = superficial velocity of the gases

$\mu$  = kinematic viscosity

Equation (5) shows that the mass transfer coefficient is generally a function of velocity of the gas in the test reactor. For lower velocities, the mass transfer boundary layer thickness is large and diffusion limits the reaction. Therefore, if there are any external mass transfer resistances present in the system, the conversion obtained for lower flow rates would be less for the same mass to flow rate ratio. The experiments were performed with pellets pressed under a force of 0.5 ton and attached to a stainless steel strip. The following results were obtained:

TABLE 10. EFFECT OF FLOW RATE ON REACTION RATE AT CONSTANT SPACE VELOCITY (BATCH D)

Experiment	Mass of the catalyst (g)	Flow rate (cm <sup>3</sup> / min)	Space velocity (cm <sup>3</sup> /g.s)	Conversion (%)
1	0.2	70	5.8	15
2	0.1	35	5.8	14

The results obtained above justifies our assumption of negligible external mass transfer resistances in the test reactor.

### 3.2.4.2. EXPERIMENTS TO DETERMINE APPARENT REACTION RATE

#### ORDER:

The following experiments were performed at room temperatures.

TABLE 11. EFFECT OF SPACE VELOCITY ON APPARENT REACTION RATE  
AT CONSTANT TEMPERATURE (BATCH D)

Experiment	Mass of the catalyst (g)	Flow rate (cm <sup>3</sup> /min)	Space velocity (cm <sup>3</sup> /g.s)	Conversion (%)
1	0.21	70	5.6	9
2	0.21	35	2.8	12
3	0.21	11	0.9	30

The powdered form of the catalyst fit the first-order plug-flow equation. In the case of pellets we expect that internal diffusion resistances may be present. However, the apparent reaction order would still remain first order in that case (1). Figure 6 shows a plot of  $-\ln(1-x)$  vs  $1/q$  for the pellets. The data fits the straight line reasonably well.

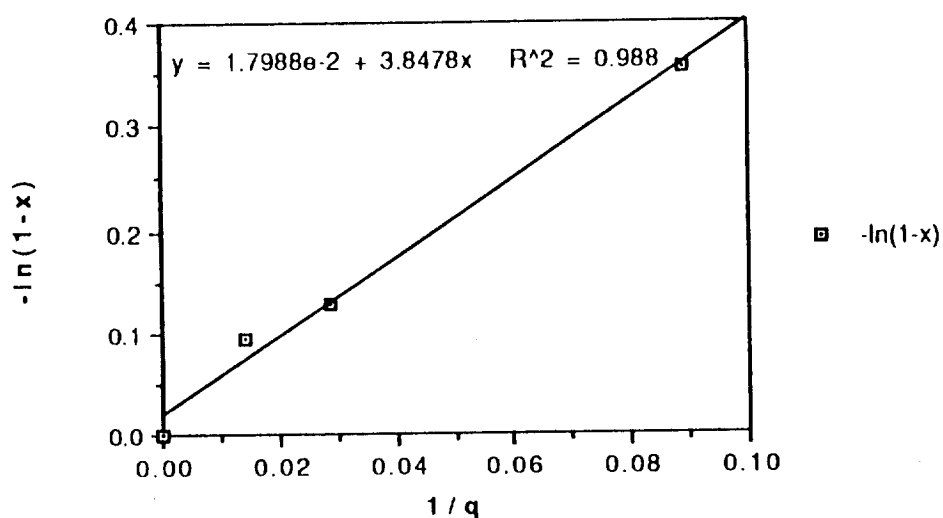


Figure 6. First-order fit for Au/MnO<sub>2</sub> pellets

### 3.2.4.3. EXPERIMENTS TO DETERMINE THE APPARENT ACTIVATION ENERGY:

The experiments to determine apparent activation energy were performed at flow rates of 70 cm<sup>3</sup>/min and a space velocity of 5.6 cm<sup>3</sup>/g.s.

TABLE 12. EFFECT OF TEMPERATURE ON THE REACTION RATE AT CONSTANT SPACE VELOCITY (BATCH D)

Experiment	Mass of the catalyst (g)	Temperature (°C)	Conversion (%)
1	0.21	23	9
2	0.21	38	17
3	0.21	49	25

In addition to an apparent reaction order, there is also an apparent activation energy,  $E_{app}$  (1). This is the activation energy one would calculate, using the experimental data, from the slope of a plot of  $\ln k$  as a function of  $1/T$  at a fixed concentration of A. From Figure 7 the apparent activation energy of the reaction is found to be 2.9 kcal/mol, which is one-half the true activation energy (5.7 kcal/mol) obtained from Figure 5.

The first-order rate equation is

$$-r = k_{app} [CO]_s = \Omega k_{true} [CO]_s \quad (6)$$

where

$$k_{app} = A_{app} \exp(-E_{app} / RT) \quad (\text{Measured, Apparent}) \quad (7)$$

$$k_{true} = A_{true} \exp(-E_{true} / RT) \quad (\text{True}) \quad (8)$$

$$\Omega = \frac{\text{actual overall rate of reaction}}{\text{rate of reaction that would result if the entire interior surface were exposed to the external pellet surface concentration } [CO]_s} \quad (9)$$

For the case of strong internal diffusional resistance, the effectiveness factor  $\Omega$  is

$$\Omega = 1 / \phi = (1 / L) (D_e / k_{true})^{1/2} \quad (10)$$

where  $\phi$  is the Thiele modulus. Substituting Equations (7 - 10) into Equation (6), we obtain:

$$A_{app} \exp(-E_{app} / RT) = (D_e^{1/2} / L) A_{true}^{1/2} \exp(-E_{true} / 2RT) \quad (11)$$

Assuming that  $D_e$  varies negligibly with temperature, this results in:

$$A_{app} = (D_e^{1/2} / L) A_{true}^{1/2} \quad (12)$$

and

$$E_{app} = E_{true} / 2$$

(13)

which corresponds to the result that we obtained above.

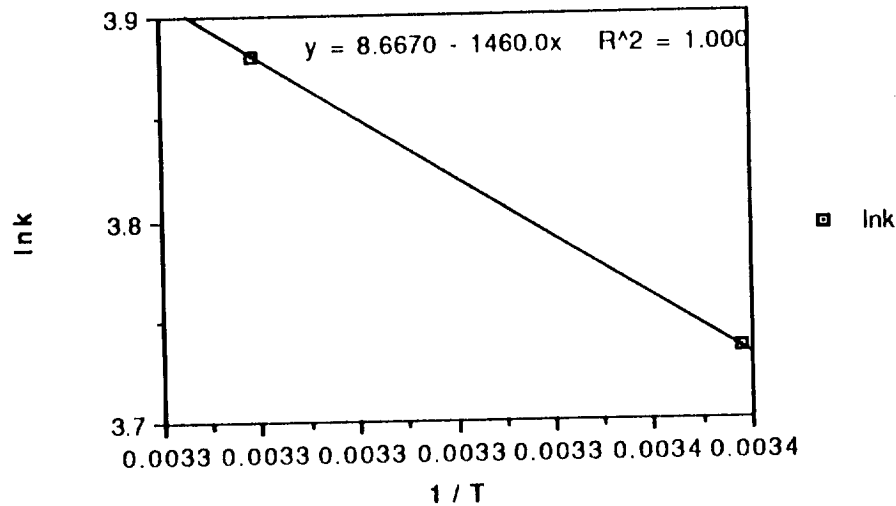


Figure 7. Activation energy for Au/MnO<sub>2</sub> pellets

#### 3.2.4.4. THIELE MODULUS ANALYSIS:

The activity tests on pellets were performed on various configurations: pellets attached to stainless steel strip (ES), pellets with epoxy applied to one side of the pellets without being attached to the stainless steel strip (ENS), and simple pellets (NENS). All experiments were performed at room temperature using flow rates of 70 cm<sup>3</sup>/min. All the pellets were pressed under a force of 0.5 ton, except where noted otherwise. The results obtained are as follows:

TABLE 13. EFFECT OF EPOXY AND STAINLESS STEEL STRIP ON  
REACTION RATE (BATCH B)

Experiment	Configuration	Mass of the catalyst (g)	Pellet thickness (mm)	Conversion (%)
1	NENS	0.22	1.1	31
2	ENS	0.23	1.1	22
3	ES	0.22	1.1	12
4	ES	0.23	1.1	13
5	NENS	0.22	2.0	21
6	NENS	0.22	2.0	22
7	ES	0.25	2.0	18
8	ES	0.24	2.0	16

The table below gives the true and apparent reaction rate constants calculated by using the isothermal first-order equation.

TABLE 14. EFFECT OF EPOXY, STAINLESS STEEL STRIP AND THICKNESS OF THE PELLET ON THE TRUE AND APPARENT REACTION RATE CONSTANT (BATCH B)

Configuration (thickness (mm))	$k_{\text{true}}$ ( $\text{cm}^3/\text{g}\cdot\text{s}$ )	$k_{\text{apparent}}$ ( $\text{cm}^3/\text{g}\cdot\text{s}$ )
POWDER	4.6	-----
NENS (1.1)		1.97
ENS (1.1)		1.26
ES (1.1)		0.68
NENS (2.0)		1.25
ES (2.0)		0.93

The conversion obtained for the pellets was found to be less than the powdered form of the catalyst under similar conditions of flow rates and temperature. The lower activity of the pellets is due to the internal resistance to diffusion of reactants. When the reactants diffuse through into the pores within the catalyst pellet, the concentration at the pore mouth will be higher than that inside the pore, and the entire catalytic surface is not exposed to the same concentration. Therefore the apparent reaction rate is product of the effectiveness factor  $\Omega$  and the reaction rate with all active surface exposed to  $[\text{CO}]_s$ :

$$-r = \Omega k_{\text{true}} [\text{CO}]_s \quad (14)$$

The effectiveness factor for a semi-infinite slab-geometry pellet is given by:

$$\Omega = \frac{\tanh(\phi)}{\phi} \quad (15)$$

The Thiele modulus for this case is

$$\phi = \frac{L}{\sqrt{\frac{k_{true}}{D_e}}} \quad (16)$$

where

$L$  = characteristic diffusion length = half-thickness of semi-infinite slab

$D_e$  = effective diffusivity

Effective diffusivity accounts for the facts that:

1. Not all the area normal to the direction of the flux is available for the molecules to diffuse.
2. The path is tortuous.
3. The pores are of varying cross-sectional area.
4. Diffusion in small pores occurs by Knudsen diffusion.

The experimental effectiveness factor for the various configurations is defined as (1):

$$\Omega = \frac{k}{k_{true}} \quad (17)$$

where the value of  $k$  was determined from Equation (3) for various configurations, and the value of  $k_{true}$  was determined from Equation (2) with the experiments performed with the powdered form of the catalyst. The data obtained from configuration NENS for pellets having a thickness of 1.1 mm was used to calculate the experimental effectiveness factor for that configuration using Equation (17), which is correct for a semi-infinite slab-geometry pellet but which is an approximation for our finite pellets. This experimental effective-

ness factor was then used to determine the Thiele modulus ( $\phi$ ) for that configuration (NENS) from Equation (16). Then an appropriate characteristic diffusion length,  $L$ , for the actual pellet was calculated from:

$$L = \frac{\text{volume of the pellet}}{\text{external geometric surface area of the pellet exposed to the flowing gas}} \quad (18)$$

For the NENS configuration, this is:

$$L = \frac{\pi R^2 T}{2 (\pi R^2 + \pi R T)} \quad (19)$$

where,

$T$  = thickness of the pellet

$R$  = radius of the pellet

Assuming the effective diffusivity is independent of the thickness and density of the pellets and pressing force of the pellets, the theoretical Thiele modulus for configurations other than NENS can be determined using equation:

$$\frac{\phi \text{ (other configurations)}}{\phi \text{ (NENS)}} = \frac{L \text{ (other configurations)}}{L \text{ (NENS)}} \quad (20)$$

For the pellets epoxied to the stainless steel strip it was assumed that no diffusion takes place through one of the faces of the pellets and, hence, the characteristic diffusion length for such configurations was taken as:

$$L = \frac{\pi R^2 T}{(2 \pi R T + \pi R^2)} \quad (21)$$

Once the Thiele modulus was obtained for a particular configuration, the effectiveness factor was calculated using Equation (15). The results from the above calculations are summarized below:

TABLE 15. COMPARISON OF THEORETICAL EFFECTIVENESS FACTOR  
WITH THE EXPERIMENTAL EFFECTIVENESS FACTOR  
(BATCH B)

Configura- tion	Diffusion length (mm)	$\phi$ (Thiele mod.)	Thick- ness of the pellet (mm)	Theoret- ical $\Omega$	Experimen- tal $\Omega$	Error (%)
NENS	0.35	2.25	1.1	set = 0.44	0.44	set = 0
NENS	0.50	3.17	2.0	0.31	0.28	10
ES	0.66	4.18	2.0	0.24	0.23	4
ENS	0.53	3.29	1.1	0.30	0.28	6
ES	0.53	3.29	1.1	0.30	0.15	50
ES (corrected)	0.53	7.04	1.1	0.14	0.15	7

The only configuration for which the experimental effectiveness factor does not agree with the theoretical effectiveness factor is the ES configuration. The low Thiele modulus for this case is due to assumption that the diffusion takes place through the edges of the pellets. Closer examination of the sample showed that epoxy covered the edges of the pellet with the result that no diffusion took place through them. The corrected ES configuration takes into account that no diffusion takes place through the edges, and the theoretical value of the effectiveness factor matches well with the experimental value.

In the table given below the theoretical effectiveness factor found above was used to calculate the conversion from the first-order plug-flow equation:

$$-\ln(1-x) = \Omega k_{\text{true}} (W/q) \quad (22)$$

The conversion obtained was then compared to the experimental conversion obtained during the activity test. The results are given below:

TABLE 16. COMPARISON OF THEORETICAL CONVERSION WITH  
EXPERIMENTAL CONVERSION (BATCH B)

Configura tion	Diffusion length (mm)	$\phi$ (Thiele modulus)	Thick- ness (mm)	Theoret- ical con- version	Experi- mental con- version	Er- ror (%)
NENS	0.35	2.25	1.1	set = 31	31	set = 0
NENS	0.50	3.17	2.0	23	21	8
ES	0.66	4.18	2.0	18	18	2
ENS	0.53	3.29	1.1	24	22	6

The results above show that the theoretical conversion corresponds well with the experimentally obtained conversion.

The effective diffusivity of the reactants within the pellet is given by:

$$D_e = \frac{L^2 k_{true}}{\phi^2} \quad (23)$$

The value of the effective diffusivity was found to be  $2.3 \times 10^{-3} \text{ cm}^2/\text{s}$ . The obstruction free molecular diffusivity of the reactants in  $\text{N}_2$  using the Chapman Enskog equation gives a value of  $0.14 \text{ cm}^2/\text{s}$ . The obstruction free molecular diffusivity is related to the effective diffusivity by (39):

$$D_e = D_{AB} f_\epsilon (\epsilon / \tau) \quad (24)$$

where:

$D_{AB}$  = molecular diffusivity

$f_\epsilon (\epsilon / \tau)$  = correction factor

$\epsilon$  = pellet porosity = (volume of void space) / (total volume)

$\tau$  = tortuosity

The simplest form of the correction factor obtained by Feng and Stewart is


$$f_\epsilon = \epsilon / 3 \quad (25)$$

The value of  $f_\epsilon$  calculated from our data is 0.016, which gives the porosity of the pellet to be 0.05. This value is compared below to another estimate of porosity.

## BATCH D

Experiments on this batch of catalyst was performed on various configurations. All experiments were performed at room temperature and using reactant flow rate of 70 cm<sup>3</sup>/min. The following results were obtained:

TABLE 17. EFFECT OF EPOXY AND STAINLESS STEEL STRIP ON REACTION RATE (BATCH D)

Experiment	Configuration	Mass of the catalyst (g)	Conversion (%)
1	ES (0.5 ton, epoxy applied to the outer circumference of the face attached to the strip). In cross-section: 	0.2	12
2	ENS (0.5 ton, epoxy applied to the entire face of the pellet)	0.2	12
3	NENS (0.5 ton)	0.2	17
4	NENS (1.0 ton)	0.2	16
5	NENS (1.5 ton)	0.2	16

The results above show that the epoxy did not penetrate the pellet and the epoxy and the stainless steel strip had the same effect on the pellet activity. The force under which the pellet was pressed had little effect on the activity of the pellet.

The table below gives the true and apparent reaction rate constants calculated by using the isothermal plug-flow first-order equation.

TABLE 18. EFFECT OF PELLETIZING FORCE ON TRUE AND APPARENT REACTION RATE CONSTANTS (BATCH D)

Configuration	$k_{\text{true}}$ (cm <sup>3</sup> /g·s)	$k_{\text{apparent}}$ (cm <sup>3</sup> /g·s)
POWDER	4.7	-----
NENS (0.5 ton)	-----	1.09
NENS (1.0 ton)	-----	1.01
NENS (1.5 ton)	-----	1.01
ES (0.5 ton)	-----	0.74
ENS (0.5 ton)	-----	0.74

The table below gives the Thiele modulus and the experimental and theoretical effectiveness factor obtained from the data.

TABLE 19. COMPARISON OF THEORETICAL EFFECTIVENESS FACTOR  
WITH EXPERIMENTAL EFFECTIVENESS FACTOR (BATCH D)

Configu- ration	Diffusion length (mm)	$\phi$ (Thiele modulus)	Thick- ness of the pellet (mm)	Theoreti- cal $\Omega$	Experimen- tal $\Omega$	Er- ror (%)
NENS (0.5 ton)	0.50	4.2	2.0	set = 0.24	0.24	set = 0
NENS (1.0 ton)	0.49	3.9	1.8	0.24	0.22	8
NENS (1.5 ton)	0.47	3.7	1.6	0.25	0.22	12
ES (0.5 ton)	0.66	5.8	2.0	0.17	0.16	6
ENS (0.5 ton)	0.66	5.8	2.0	0.17	0.16	6

The stainless steel strip and the epoxy were found to block one of the faces of the pellet. The effective diffusivity of the reactants was found to be  $4.9 \times 10^{-3} \text{ cm}^2/\text{s}$ . The value of effective diffusivity calculated for Batch D is twice that calculated for Batch B. The pellet density of both the batches was determined to be the same.

The experimental values of the effectiveness factor obtained in Table 19 can be used to calculate the density of the solid Au/MnO<sub>2</sub> by assuming that the effective diffusivity is directly proportional to the pellet porosity that is

$$D_e \propto \epsilon \quad (26)$$

therefore

$$\theta \propto \frac{L}{\sqrt{\epsilon}} \quad (27)$$

$$\Omega \propto \frac{\sqrt{\epsilon}}{L} \quad (28)$$

$$\frac{\Omega (0.5 \text{ ton})}{\Omega (1.5 \text{ ton})} = \sqrt{\frac{\epsilon (0.5 \text{ ton})}{\epsilon (1.5 \text{ ton})} \left( \frac{L (1.5 \text{ ton})}{L (0.5 \text{ ton})} \right)} \quad (29)$$

however

$$\epsilon = 1 - (\rho_{\text{pellet}} / \rho_{\text{solid}}) \quad (30)$$

where:

$\rho_{\text{pellet}}$  = density of the pellet

$\rho_{\text{solid}}$  = density of solid Au/MnO<sub>2</sub>

Since  $\rho_{\text{pellet}}$  is already known, the density of solid Au/MnO<sub>2</sub> and hence the porosity of the pellets can be calculated. The density of the solid Au/MnO<sub>2</sub> was calculated to be 11 g/cm<sup>3</sup>. This density for the co-precipitated catalyst is greater than the density of 6 g/cm<sup>3</sup> for an equivalent amount of solid Au and solid MnO<sub>2</sub>. The porosities of the 0.5, 1.0, and 1.5 ton pellets were determined to be 0.3, 0.26, and 0.22, respectively. The fact that the values of the pellet porosity did not agree with the value of the porosity calculated by Equation

that Knudsen diffusion plays a role. The corrected values of effectiveness factors are given in Table 20.

TABLE 20. COMPARISON BETWEEN THEORETICAL AND EXPERIMENTAL EFFECTIVENESS FACTOR WITH EFFECTIVE DIFFUSIVITY CORRECTED FOR POROSITY (BATCH D)

Configu- ration	Diffusion length (mm)	$\phi$ (Thiele modulus)	Thick- ness of the pellet (mm)	Theoret- ical $\Omega$	Experimen- tal $\Omega$	Er- ror (%)
NENS (0.5 ton)	0.50	4.2	2.0	set = 0.24	0.24	set = 0
NENS (1.0 ton)	0.49	3.9	1.8	0.23	0.22	4
NENS (1.5 ton)	0.47	3.7	1.6	set = 0.22	0.22	set = 0

The theoretical effectiveness factor for the 1.0 ton pellet was found to be closer to the experimentally obtained effectiveness factor when the effective diffusivity was assumed to be directly proportional to pellet porosity (4% error), relative to the case when effective diffusivity was assumed to be independent of the pellet porosity (8% error).

In the table given below, the theoretical effectiveness factors found above for the case of constant diffusivity was used to calculate the conversion from

Equation (22). The conversion obtained was then compared to the experimental conversion obtained during the activity test.

TABLE 21. COMPARISON BETWEEN THEORETICAL CONVERSION AND EXPERIMENTAL CONVERSION (BATCH D)

Configura- tion	Diffu- sion length (mm)	$\phi$ (Thiele modu- lus)	Thickness of the pellet (mm)	Theoret- ical con- version	Experimen- tal conver- sion	Error (%)
NENS (0.5 ton)	0.5	4.2	2.0	set = 17	17	set = 0
NENS (1.0 ton)	0.49	3.9	1.8	17	16	6
NENS (1.5 ton)	0.47	3.7	1.6	16	15	6
ES (0.5 ton)	0.66	5.8	2.0	14	15	7
ENS (0.5 ton)	0.66	5.8	2.0	14	14	7

The theoretical conversion calculated is found to be in good agreement with the experimental conversion.

Besides these batches of catalyst, another batch of catalyst was also used. This batch of catalyst powder showed far lesser activity than the other batches and also showed a decline in activity with time, as shown in Figure 8. All the

other batches of the catalyst showed constant activity over a 5-8 hour period. The BET surface area ( $65 \text{ m}^2/\text{g}$ ) of this batch of catalyst was found to be less than Batches B and D. Since no records were maintained by the personnel who made this batch of catalyst, the actual cause of the low activity and decline in the activity is not known. However experiments with unwashed catalyst and catalyst washed with cold water (6) have shown far lower activity compared to catalysts that were washed with hot water. Another possible reason for the lower activity of this batch could be overheating of the catalyst during calcination resulting in collapse of pore walls. The crush strength of this batch of catalyst was found to be less than Batch D.

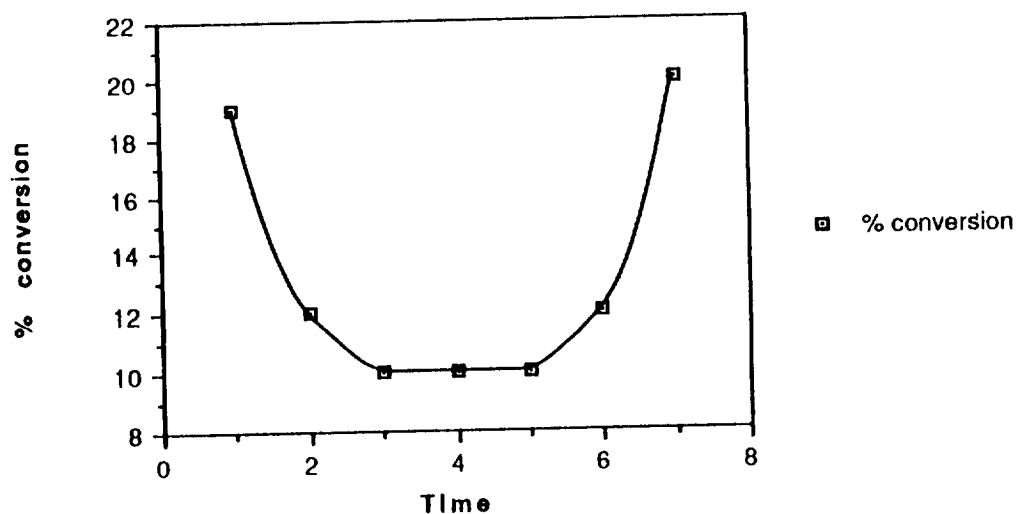


Figure 8. Variation of conversion with time for bad batch of catalyst:  $40^\circ\text{C}$ ,  $0.2 \text{ g}$ ,  $11.5 \text{ cm}^3/\text{min}$  (STP).

#### 4. **CONCLUSIONS:**

The CO oxidation reaction over Au/MnO<sub>2</sub> powder was found to be first order overall, and the true reaction rate constant at room temperature for Batches B, C and D were found to be 4.6, 4, 4.7 cm<sup>3</sup>/g·s, respectively. The reaction rate constant for 1.8 % Pd/SnO<sub>2</sub> was found by Stark and Harris to be  $8.2 \times 10^{-2}$  cm<sup>3</sup>/g·s (43), approximately 60 times lower. The true activation energy of the reaction over the catalyst was determined to be 5.7 kcal/mol (23 kJ/mol). The activation energy of CO oxidation reaction over 1.3 % Pt/SnO<sub>2</sub> and 1.8 % Pd/SnO<sub>2</sub> is 9.9 and 9.5 kcal/mol, respectively (43), approximately twice the value for Au/MnO<sub>2</sub>.

BET surface area measurements could not be performed on the powdered form of the catalyst. The diffusional resistance for the gas desorbing from the powder was minimal resulting in large amounts of gas being desorbed in a short interval of time and leading to saturation of the instruments. BET surface area experiments performed on pellets showed that the pelletizing force had no effect on the surface area of the pellet. The surface area for Batches B and D was found to be 150 m<sup>2</sup>/g and 126 m<sup>2</sup>/g respectively.

Pellets 4 mm in diameter and from 1.1 to 2 mm thick were pressed from Au/MnO<sub>2</sub> powder. Pellets epoxied to stainless steel strip showed no sign of fracture or dusting when subjected to the thermal test. Pellets can be dropped onto a hard surface with chipping of edges but not breakage of the pellets. The density of the pellets increased with increasing pelletizing force. Mechanical strength tests performed on pellets pressed under different pelletizing forces showed that the crush strength increased from 250 lbs to 750 lbs as the pelletizing force increased from 1000 lbs to 3000 lbs. The crush strength is roughly one-fourth of the pelletizing force.

Activity tests performed on the pellets showed that external mass transfer resistances were negligible over the pellets. The apparent activity of the pellets was found to be less than that of the powdered form of the catalyst. The lower apparent activity of the pellets is due to fact the internal surface area of the pellet was not exposed to the reactant concentration present in the flowing gas as a result of intrapellet diffusion resistance. The apparent reaction rate was determined to be first-order. The apparent activation energy was found to be 2.9 kcal/mol, which is approximately one-half of the true activation energy. The variation of the apparent activation from the true activation energy was explained by accounting for the intrapellet diffusion resistance.

Effectiveness factors varied from 0.44 for pellets having a thickness of 1.1 mm with both faces exposed to the gas, to 0.15 for pellets having thickness of 2 mm and attached with epoxy to a stainless steel strip. The epoxy and the stainless steel strip were found to simply to block off one of the circular faces of the pellets. The epoxy did not penetrate the pellets and block the active sites. The values of the effective diffusivities for Batches B and D were estimated to be  $2.3 \times 10^{-3}$  and  $4.9 \times 10^{-3}$  cm<sup>2</sup>/s, respectively. The porosity of the pellet was estimated to be 0.3, 0.26, 0.22 for pellets pressed under pelletizing forces of 0.5, 1.0, 1.5 ton, respectively. With measurements performed on one powder sample and one pellet configuration, reasonably accurate predictions can be made of conversions that would be obtained with other pellet thicknesses and configurations.

The results obtained have shown enough promise to further pursue this approach of making monolithic catalysts for CO<sub>2</sub> lasers.

## **5. RECOMMENDATIONS FOR FUTURE WORK:**

Future work on this approach to making monolithic catalysts should concentrate on more thermal and mechanical tests on the pellets. The fact that the crush strength of the pellet increases with the pelletizing force without having much effect on the effective diffusivity of the pellet suggests that pellets with higher crush strength can be used in the lasers without any compromise on the activity. However extensive mechanical and thermal tests need to be carried out before coming to any decision. One of the ways of increasing the strength of the pellet is to add binders to the catalyst. Therefore the effect of various binders on the strength and the activity of the pellets should be examined. Another question that needs to be investigated is whether the epoxy is compatible with laser gases, that is, does it outgas and effect the laser performance or not. Therefore the pellets attached to the stainless steel strip need to be tested in the laser.

The performance of the catalyst should be measured in presence of  $\text{CO}_2$ . Activity tests in this work were carried out in presence of stoichiometric mixtures of CO and  $\text{O}_2$  which do not stimulate the conditions inside the laser, where the concentration of  $\text{CO}_2$  exceeds the concentration of CO and  $\text{O}_2$ .

The performance of  $\text{Au/MnO}_2$  should be compared with the performance of other catalysts in consideration for the  $\text{CO}_2$  lasers such as  $\text{Pt/SnO}_2$ . The performance of the catalyst should also be observed by adding additives that would increase the effective diffusivity of the reactants inside the pellets. The performance of an untreated catalyst should be compared with a catalyst that is pretreated in a reducing atmosphere, in order to understand the effect of pretreatment on the activity of the catalyst.

As heterogeneous catalysis is a surface phenomenon, the determination of surface properties plays an important role in catalyst characterization and in understanding the reaction mechanism. Once the surface intermediates are known by various surface characterization techniques, the reaction mechanism can be understood leading to better reactor and catalyst design.

Alternatives other than pellets should also be considered, such as extrusions and granules. Extrusions have the advantage that they have a usually long irregular shape of larger external surface area. They are less dense than the pellets and hence have less internal diffusion resistance. The advantage of using granules is that they have a larger external surface area (spherical shape) and are less dense than the pellets. However both granules and extrusions have less mechanical strength to withstand attrition than pellets. A comparative study of performance of the catalyst in different forms can lead to further insights on catalyst performance.

## 6. REFERENCES:

1. Fogler, S., "Elements of Chemical Reaction Engineering", Prentice-Hall, New Jersey (1986).
2. Witteman, "The CO<sub>2</sub> laser", Springer-Verlag, New York (1987).
3. Burton, J.J., Garten R.L., "Advanced Materials in Catalysis", Academic Press (1977).
4. Upchurch, B.T., Miller I.M., Kielin E.J., "Rare isotope and kinetic studies of Pt/SnO<sub>2</sub> catalysts", NASA conference publication 3076, 193-197 October (1989).
5. Van Norman, J.D., Brown, K.G., Schryer, J., "The Effect of H<sub>2</sub>O and pre-treatment on the activity of Pt/SnO<sub>2</sub> catalyst NASA conference publication 3076, 181-191 October (1989).
6. Gardener, S.D., Hoflund, G.B., "Alternative catalysts for low temperature CO oxidation" NASA conference publication 3076, 123-135 October (1989).
7. Guinn, K., Noskowski, E., Herz, R.K., "A computer program for the design of catalytic monoliths for CO<sub>2</sub> lasers." NASA conference publication 3076, 139-154 October (1989).
8. Carts, Y.A., "CO<sub>2</sub> lasers serve in advanced remote sensing studies", Science, 71-82 (1990).
9. Higginson, W.G., "Making Catalysts - An overview" Chemical Engineering 98-104 (1974).
10. Haruta, M., Kobayashi, T., Sano, H., Yamada, N., "Novel Gold catalyst for oxidation of CO at temperature far below 0°C", Chemistry Letters, 405-408 (1987).

11. Haruta, M., Kageyama, H., Kamijo, N., Kobayashi, T., Delannay, F., "Fine structure of novel gold catalysts prepared by coprecipitation", *Successful Design of Catalysts*, 33-42, Elsevier Science Publishers, Amsterdam (1988).
12. Haruta, M., Yamada, N., Kobayashi, T., Iijima, S., "Gold catalysts prepared by coprecipitation for low temperature oxidation of hydrogen and of CO", *Journal of Catalysis* 115, 301-309 (1989).
13. Twigg, M. V., "Catalyst Handbook", Wolfe Publishing Ltd, England (1989).
14. Andrew, S.P.S., "The black art of designing and making catalysts", *Chemtech*, 180-184 (1979).
15. Herz, R.K., "Low temperature CO oxidation over noble metal reducible oxide catalysts" NASA conference publication 3076, 21-31 October (1989).
16. Herz, R.K., "Chemical Engineering design of CO oxidation catalyst", NASA conference publication 2456, 103-112 June (1986).
17. Levenspiel, O.P., "Chemical Reaction Engineering," 2nd Ed., John Wiley & Sons (1972).
18. Willetts, D.W., "Pulsed Discharge Carbon dioxide Lasers", NASA conference publication 3076, 3-19 October (1989).
19. Klier, K., Kuchynka, K., "Carbon Monoxide oxidation and Adsorbate-Gas Exchange Reactions on MnO<sub>2</sub> based catalysts", *Journal of Catalysis* 6, 62-71 (1966).
20. Yates, D.J., *Colloid Interface Science*, 29, 194 (1969).
21. Lam, Y.L., and Boudart, M., *Journal of Catalysis* 50, 530 (1977).

22. Nyarady, S.A., and Sievers, R.E., Journal of American Chemical Society 107 (1985).
23. Sermon, P.A., Bond, G.C. and Wells, P.B., Journal of American Chemical Society 74, 3726 (1978).
24. Galvagno, S. and Parravano, G., Journal of Catalysis, 55, 178 (1978).
25. Fukushima, T., Galvagno, S., and Parravano, G., Journal of Catalysis 57, 177 (1979).
26. Lea, J.Y., and Schwank, J., Journal of Catalysis, 102, 207 (1979).
27. Buchanan, D.A., and Webb, G., Journal of Chemical Society 70, 134 (1974).
28. Schwank, J., Parravano, G. and Gruber, H.L., Journal of Catalysis ,61, 19 (1980).
29. Shastri, A.G., Datye, A.K and Schwank, J., Journal of Catalysis 87, 265 (1984).
30. Chapman, D.L., Ramsbottom, J.E., and Trotman, C.G., Proc. Soc. London A, 107, 29 (1925).
31. Benton, A.F., and Elgin, J.C., Journal of American Chemical Society, 49, 2426 (1927).
32. Chambers, R.P., and Boudart, M., Journal of Catalysis, 5, 517 (1966).
33. Cant, N.W., and Fredrickson, P.W., Journal of Catalysis, 37, 531 (1975).
34. Bollinger, M.J., Sievers, R.E., Fahey, D.W., and Fehsenfeld, F.C., Analytical Chemistry, 55, 1980 (1983).
35. Hodges, C.N., and Roselaar, L.C., Journal of Applied Chemical Biotechnology , 25, 609 (1975).
36. Bond, G.C., Gold Bulletin, 5, 11 (1972).
37. Handbook of laboratory safety, CRC Press, Boca Raton FL (1985).

38. Thomas, J.M., Thomas, W.J., "Introduction to the principles of heterogeneous catalysis", Academic Press, New York (1975).
39. Lee, H.H., "Heterogeneous Reactor Design", Butterworth Publishers, Boston (1985).
40. Kays, W.M., Crawford, M.E., "Convective Heat and Mass transfer", McGraw-Hill, New York (1980).
41. Shah, R.K., and London, A.L. Tech. Rep. #75, Department of Mechanical Engineering, Stanford University, Stanford California. (1971).
42. Carberry, J.J, Kulkarni, A.A., Journal of Catalysis 31, 41 (1973).
43. Stark, D.S., and Harris, M.R., "Catalyzed recombination of CO and O<sub>2</sub> in sealed CO<sub>2</sub> TEA laser gases at temperatures down to -27°C", J. Phys.E: Sci Instrum., 16, 492-496 (1983).

## 7. APPENDIX:

### 7.1. BET TOTAL SURFACE AREA MEASUREMENTS:

#### 7.1.1. PROCEDURE:

BET experiments are performed to determine the exposed surface area of catalysts. Before starting with the BET experiments the catalyst whose surface area has to be determined is degassed. The degassing process requires the sample to be heated in flowing He to 200°C for approximately 20 min and then maintaining the temperature at 200°C for another 20 min in flowing He. The sample is then allowed to cool to room temperature in flowing He.

In the BET experiments performed the adsorbate used was Kr because of its lower  $p_0$  value (2.0 Torr) as compared to  $N_2$  (760 Torr) at liquid  $N_2$  temperature. A stream of gas composed of adsorbate and inert carrier is passed through a previously degassed catalyst and the concentration of the adsorbate monitored frequently by a thermal conductivity cell. Conditions are first adjusted so that no gas will adsorb and the bridge balanced. Conditions are then adjusted so that the gas will adsorb on the sample (cooling the sample to  $LN_2$  temperatures). After sufficient time has elapsed (40-45 min for 7-8 mg samples) the sample cell is heated to desorb the Kr and the change in concentration of the gas is monitored by the thermal conductivity detector. The signal is then passed on to an amplifier that magnifies the input by ten times and transmits the output to a Macintosh Analog Digital Input Output System (MacADIOS) model 411. The data collected by the MacADIOS is passed on to a Macintosh Plus through a program written in Quick BASIC.

Another program in Quick BASIC then analyses the data obtained and integrates the area under the peak and hence determines the surface area of the sample. The thermal conductivity detector was calibrated using aluminium oxide gamma pellets (Alfa products) having a surface area of 100 m<sup>2</sup>/g. The pellets were made by pressing the catalyst powder under forces of 0.5, 1.0, 1.5, 2.0 ton.

### 7.1.2. COMPUTER PROGRAMS:

#### PROGRAM 1

```

LIBRARY "411Drivers Interface"
LIBRARY "DataManipulation Interface"
CALL mainit
DIM a%(24000)
CALL msinit(4,1,4999,1)
CALL ainx(1,0,23999,0,0,VARPTR(a%(0)),0,0,0,0,0)
PRINT "Enter name of new output file"
LINE INPUT OUTF$
OPEN OUTF$ FOR OUTPUT AS #1
FOR n = 0 TO 23999
    PRINT #1,n a%(n)
NEXT n
CLOSE #1
PRINT "Next step is to input file and compare"
PRINT "Hit <RETURN> to continue"
LINE INPUT instring$

```

```
INF$ = FILES$(1,"TEXT")
PRINT "Input file is ";INF$
OPEN INF$ FOR INPUT AS #1
FOR n = 0 TO 23999
    INPUT #1,n, a%(n)
    PRINT n,a%(n)
NEXT n
CLOSE #1
STOP
```

## PROGRAM 2

```
LIBRARY"411Drivers Interface"
LIBRARY"DataManipulation Interface"
DIM a%(24000)
OPEN "FILE NAME" FOR INPUT AS #1
WHILE NOT EOF(1)
    FOR n = 0 TO 23999
        INPUT #1,n,a%(n)
    NEXT n
WEND
sum1! = 0
FOR n = 0 TO n
    sum1! = a%(n)+sum1!
NEXT n
avg1! = sum1!/n
sum2! = 0
```

```
FOR n = n TO k
sum2l = sum2l+a%(n)
NEXT n
integ1l = sum2l-(n-k)*baseline
PRINT "THE PEAK AREA IS ",integ1l
sum3l = 0
FOR n = k+1 TO 23999
sum3l = sum3l+a%(n)
NEXT n
avg2l = sum3l/23999-(k+1)
PRINT"THE AVERAGE B.L. VALUE BEFORE THE PEAK IS"avg1l
PRINT"THE AVERAGE B.L. VALUE AFTER THE PEAK IS"avg2l
larl=100
FOR n = 0 TO 23999
IF (larl<a%(n)) THEN larl=a%(n)
NEXT n
PRINT "THE LARGEST VALUE IN THE ARRAY IS"larl
match = integ1l/integ2l
PRINT"THE RATIO OF THE TWO PEAK AREAS IS"match
shiftl = (avg1l-avg2l)/(larl-avg2l)
PRINT"THE BASE LINE SHIFT IS" shiftl
CALL plot(0,0,200,300,VARPTR(a%(n)),120,180,300,1,0,1,0)
STOP
```

## 7.2. CO OXIDATION REACTOR:

### 7.2.1. ROUTINE OPERATIONS:

1. Installing new catalyst sample:

Purge the entire reactor cabinet with  $N_2$  for about 12 min. Open fittings of the reactor to change the catalyst.

2. Changing CO Cylinders:

Purge the entire reactor and the gas cabinet with  $N_2$  and then remove the pressure gauge and change the cylinders.

3. Calibrating the system:

With the power off verify that the front panel reading of the IR analyzer reads zero. Apply power and turn the range switch to tune. Allow the analyzer to warm up for at least one hour and preferably for 8 hours. Turn range switch to position 1. Pass zero gas ( $N_2$ ) to the sample inlet and adjust the zero control on the front panel so that it reads zero in all three range positions. Now connect the upscale gas (1%  $CO_2$  +  $N_2$ ) to the inlet of the IR analyzer. Turn on the  $CO_2$  cylinder and turn valve V8 to position 1 ( $CO_2$  flow) and valve V9 to position 2. Verify that the Range switch is in position 1 and adjust the gain control on the front panel so that the meter reads 100. The value of on the meter when CO is passed through the system gives the conversion of CO to  $CO_2$ .

4. Installing catalyst in Reactor II:

Purge the lines between the reactor cabinet and gas cylinder cabinet.

Open the fittings of the reactor and change the catalyst.

5. End of the day shutdown:

Purge lines between the gas cylinder cabinet and the reactor cabinet.

Shut off the flow of  $N_2$  when the entire system has been purged. If the system is left running overnight then a sign on the door should be stuck explaining the danger if the alarm is sounding.

7.2.2. EMERGENCY PROCEDURES:

1. REACTOR I FAILURE WHILE CO IS FLOWING THROUGH THE SYSTEM:

In case of reactor failure (fittings becoming loose or development of leaks) follow instructions on how to purge the gas regulator, turn valve V6 to position 2 (shut off) and turn valve V7 to position 2 (shut off).

When the reactor is fixed start the flow of  $N_2$  through the system and check for possible leaks in the reactor fittings. Start the flow of CO only after making sure that there are no leaks in the system. Start the flow of CO through the system by turning valve V7 to position 1 (CO flow) and turning valve V6 to position 1 (to reactor).

## 2. EXHAUST FAN NOT WORKING:

When the exhaust fan is not working turn valve V6 to position 2 (shut off) and valve V5 to position 2 (shut off). Turn valve V7 to position 2 (shut off) so that all flow to the reactor is stopped. The alarm system would automatically shut off the solenoid valve.

## 3. LEAKS IN THE SYSTEM:

As soon as leaks are detected in the system by the CO detector the alarm would go on and solenoid valve shut off. As soon as the alarm goes on turn valve V5 to position 1 (to vent) and valve V6 to position 2 (shut off). Get all the people out of the lab, open all the lab doors and prevent anyone from entering in to the room. If the exhaust is not working then notify from Physical Plant Services and get assistance of two or more knowledgeable persons before re entering the room. After sufficient time has elapsed (for CO to disperse in the room) the cause of the leak should be determined and the leak fixed. N<sub>2</sub> should then be passed through the system to make sure that there are no leaks present in the system.